SANDIA REPORT SAND86-8007 • Unlimited Release • UC-62a
Printed March 1986

An Evaluation of Heliostat Field/Receiver Configurations

S. E. Faas and W. S. Winters

Prepared by
Sandia National Laboratories
Albuquerque, New Mexico 87185 and Livermore, California 94550
for the United States Department of Energy
under Contract DE-AC04-76DP00789

Issued by Sandia National Laboratories, operated for the United States Department of Energy by Sandia Corporation.

Printed in the United States of America
Available from
National Technical Information Service
5285 Port Royal Road
Springfield, VA 22161

NTIS price codes
Printed copy: **A04**
Microfiche copy: A01

SAND86-8007
Unlimited Release
Printed March 1986

UC-62a

AN EVALUATION OF HELIOSTAT FIELD/RECEIVER CONFIGURATIONS

S. E. Faas
Solar Central Receiver Systems Division

W. S. Winters
Computational Mechanics Division

Sandia National Laboratories, Livermore

ABSTRACT

This report evaluates and compares north heliostat field/cavity receiver configurations and surround heliostat field/external receiver configurations. The receiver coolants are molten nitrate salts and liquid sodium. Both field/receiver configurations use molten salt thermal storage; the sodium receiver is thermally connected to thermal storage by a sodium-to-salt heat exchanger. The heliostat field size is fixed at 1,000,000 square meters of reflective area, and the delivered molten salt temperature is fixed at 566 ° C. The delivered thermal power varies from 500 to 600 MW_t, depending on the overall system efficiency.

The generic north heliostat field/cavity receiver configurations were found to be 6 to 10 percent more efficient than a generic surround field/external receiver configuration. There was little or no difference found in the transient performance of a molten salt receiver compared to a sodium receiver connected to a sodium-to-salt heat exchanger.

Four configurations were of particular interest: 1) a north heliostat field/single cavity molten salt receiver, 2) a surround heliostat field/external cylinder molten salt receiver, 3) a surround heliostat field/external cylinder liquid sodium receiver, and 4) a north heliostat field/single cavity liquid sodium receiver. It was found that the surround field/liquid sodium external receiver configuration may provide energy at a 14 percent lower levelized energy cost than a north field/molten salt cavity receiver configuration. However, the cost advantage of the surround field/liquid sodium external reciever is not conclusive because of uncertainties in system component costs.

FOREWORD

The research and development described in this document was conducted within the U.S. Department of Energy's (DOE) Solar Thermal Technology Program. The goal of the Solar Thermal Technology Program is to advance the engineering and scientific understanding of solar thermal technology, and to establish the technology base from which private industry can develop solar thermal power production options for introduction into the competitive energy market.

Solar thermal technology concentrates solar radiation by means of tracking mirrors or lenses onto a receiver where the solar energy is absorbed as heat and converted into electricity or incorporated into products as process heat. The two primary solar thermal technologies, central receivers and distributed receivers, employ various point and line-focus optics to concentrate sunlight. Current central receiver systems use fields of heliostats (two-axis tracking mirrors) to focus the sun's radiant energy onto a single tower-mounted receiver. Parabolic dishes up to 17 meters in diameter track the sun in two axes and use mirrors or Fresnel lenses to focus radiant energy onto a receiver. Troughs and bowls are line-focus tracking reflectors that concentrate sunlight onto receiver tubes along their focal lines. Concentrating collector modules can be used alone or in a multi-module system. The concentrated radiant energy absorbed by the solar thermal receiver is transported to the conversion process by a circulating working fluid. Receiver temperatures range from 100 ° C in low-temperature troughs to over 1500 ° C in dish and central receiver systems.

The Solar Thermal Technology Program is directing efforts to advance and improve promising system concepts through the research and development of solar thermal materials, components, and subsystems, and the testing and performance evaluation of subsystems and systems. These efforts are carried out through the technical direction of DOE and its network of national laboratories who work with private industry. Together they have established a comprehensive, goal directed program to improve performance and provide technically proven options for eventual incorporation into the Nation's energy supply.

To be successful in contributing to an adequate national energy supply at reasonable cost, solar thermal energy must eventually be economically competitive with a variety of other energy sources. Components and system-level performance targets have been developed as quantitative program goals. The performance targets are used in planning research and development activities, measuring progress, assessing alternative technology options, and making optimal component developments. These targets will be pursued vigorously to insure a successful program.

The work presented in this report was performed as part of the System Studies subelement of the Central Receiver Systems task and seeks to determine the advantages of one heliostat field/receiver configuration over competing configurations. The results of this comparison will be used in defining the work performed in the component development tasks of the Solar Central Receiver Program.

CONTENTS

ILLUSTRATIONS

TABLES

Executive Summary

It has been proposed by members of the solar community that a mid-size central receiver system of 35 to 80 MW_t utilizing a heat transfer fluid of either molten salt or liquid sodium be constructed and tested. The rationale is that a system of this size will reduce the uncertainties associated with solar thermal central receiver design and construction while costing far less than that required to construct and test a utility scale plant rated at 500 to 600 MW_t. However, it is anticipated that only one mid-sized system will be constructed. Therefore, it is necessary to examine the current state of solar central receiver technology in order to determine which of the many potential concepts is most able to meet the needs of the users in the near future. The following text presents a preliminary examination of the liquid sodium and molten nitrate salt solar central receiver technology.

In the current state of solar thermal receiver technology, there are four leading designs:

- Molten salt single cavity receiver, molten salt storage, north heliostat field.
- Molten salt external cylinder receiver, molten salt storage, surround field .
- Liquid sodium cavity receiver, molten salt storage, north field.
- Sodium external cylinder receiver with sodium-to-salt heat exchanger, molten salt storage, surround heliostat field. Sodium external receivers are predicted to cost less than molten salt cavity receivers because they are smaller in size and because they do not require an expensive cavity structure to have good thermal performance. This economy may allow a sodium receiver with molten salt storage combination to achieve a lower levelized energy cost than a molten salt system.

Evaluation Methodology

This evaluation was conducted over a two month period in order to meet internal deadlines. Therefore, the evaluation is limited in scope and covers three main issues:

1. System efficiency - the overall efficiency of the heliostat field/receiver combination at steady state will be determined. The system efficiency is defined as the product of the annual field efficiency and the design point receiver efficiency.

2. Transient performance - the startup time of each system will be determined.

3. Cost - the key system cost differences will be determined.

The first two issues allow the ability of each system to collect and absorb solar energy to be assessed. The last issue allows cost considerations to be included. The fundamental selection criterion is levelized energy cost. Since receivers are designed to a particular flux constraint based on the working fluid, system designs are discriminated from each other by the receiver peak flux capability and heat transport fluid.

System Efficiency

The conversion efficiency of solar energy to thermal energy controls the annual energy output of a solar thermal central receiver. The greater the system efficiency, the more energy is captured for a given capital investment, which in turn yields a lower delivered energy cost. The system efficiency of cavity receivers is scaled from the results of the De Laquil and Anderson study on the performance of high temperature solar central receivers[1]. The system efficiency of external receivers is calculated in a similar manner so the system efficiencies could be compared. The computer code, DELSOL2[2], developed at Sandia National Laboratories - Livermore (SNLL), was used for the heliostat field design and receiver design except where noted. An average receiver absorber surface temperature of 480 ° C was used for all receivers.

The system efficiency as a function of peak flux is shown in Figure ES-1 for a system using a heliostat field area of 10^6 m^2. The system efficiency is defined as the product of the annual field efficiency and the design point receiver efficiency. This definition of the system efficiency was used by De Laquil and Anderson and was continued in this report. The effect of this definition is to overstate the annual system efficiency since any reduction in receiver efficiency at part load is not included. It is assumed that all receivers are similarly affected by part load operation. Therefore, while the system efficiencies quoted here are not necessarily accurate on an absolute basis, they are sufficient for a relative comparison.

The most significant observation to be made from Figure ES-1 is that the cavity receiver/north field systems are about 10% more efficient than the external receiver/surround field systems. About 7 percentage points of this is due to the difference in the cosine efficiency of the two fields. This difference agrees well with that presented in a report published in 1979 by the Martin-Marietta Corporation (MMC)[3]. The remaining 3 percentage point difference in efficiency is due to the reduction in receiver radiative heat losses when a cavity structure is employed. There was little difference in the receiver convective losses.

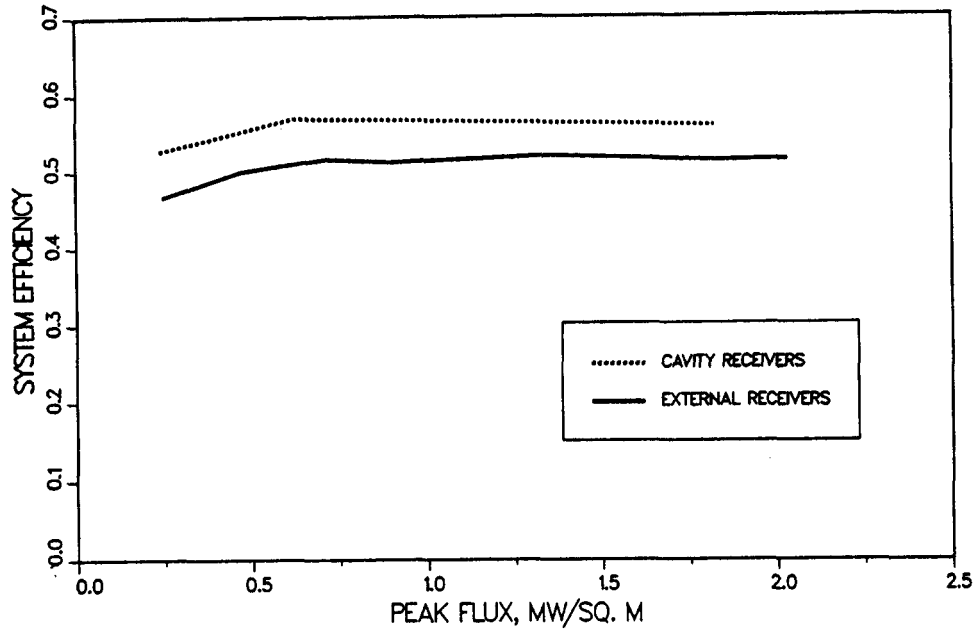

Figure ES-1. System Efficiencies

Receiver Flux Limits

It should be noted that the system efficiencies were calculated without regard to the heat transfer fluid used to cool the receiver. The selection of a heat transfer fluid controls the maximum peak flux that a tube can endure which in turn determines the maximum system efficiency. In particular, it is the heat transfer coefficient of the fluid that controls the level of thermal fatigue the receiver tubes experience and the level of thermal fatigue controls the receiver lifetime.

A linear analysis has been developed at SNLL which relates heat transfer coefficient, peak tube crown temperature, tube outside diameter, tube wall thickness, allowable strain range, and peak flux. The allowable strain range is based on ASME code case 1542 (N47). The peak allowable incident flux determined by the linear analysis is 1.02 MW_t/m^2 for a liquid sodium receiver and 0.46 MW_t/m^2 and molten salt receiver respectively. These flux values are preliminary and conservative, but do reflect the different abilities of the two fluids to cool a receiver.

Transient Performance

While the objective of the salt and salt/sodium system is to produce a steady flow of 566 ° C (1050 ° F) molten salt, the hardware configuration for the two systems suggests possible differences in the transient behavior, particularly at startup, i.e., the time required to produce steady state flow of 566 ° C salt in an initially cold system. For two systems producing hot molten salt at the same rate, one can expect the thermal mass of the sodium receiver to be substantially less

(due primarily to higher flux levels) than the salt receiver. Hence startup times for the sodium receiver should be significantly less than the salt receiver. However the sodium/salt system is handicapped at startup by the need to thermally condition (i.e., bring to steady state temperature) a potentially massive sodium-to-salt heat exchanger. This situation makes an assessment of startup times more difficult.

Numerical models have been used to compare startup times for the salt and salt/sodium systems. These models consider only the thermal inertia characteristics of the two systems. It is assumed that the rate of applying solar flux to each system is identical and that thermal conditioning of the heat exchanger occurs simultaneously with the receivers. Certain operational and/or safety considerations peculiar to one system are not addressed here, such as the need to apply flux more slowly to sodium tubes than to salt tubes (or vice versa). Furthermore, startup limitations in the receiver and heat exchanger control algorithms are not considered.

A comparison of the salt receiver and a sodium receiver connected to a sodium to salt heat exchanger is shown in Figure ES-2. The solar flux is applied to the receivers increasing from zero to full flux over a 10 minute period. Two sodium receiver/heat exchanger systems are presented; one uses a heat exchanger with a fast thermal response characteristic and the other uses a heat exchanger with a slow response. The combination of heat exchanger design parameters determines the heat exchanger thermal response. The "fast" and "slow" heat exchanger designs are based on numerous parametric studies and represent the extremes in performance.

The fast sodium/salt system responds more quickly than the salt system in the early time period. This is due primarily to the initial conditions selected for the heat exchanger and the inventory of 315 ° C (600 ° F) sodium available for raising the salt temperature from 288 ° C (550 ° F) to 315 ° C before significant heat flux is applied. However, the overall rate of salt temperature rise is nearly the same for all systems. This is because the thermal inertia and lower heat transfer of molten salt are the controlling factors in all system responses.

Since the salt and sodium/salt systems have similar transient responses, it will not be necessary to account carefully for the effects of plant startup on the collected annual energy when making relative comparisons between these two systems.

Economic Comparison

The system efficiency and system transient performance serve to establish the annual energy output of a particular system configuration. However, the value of a solar central receiver plant is determined by its levelized energy cost.

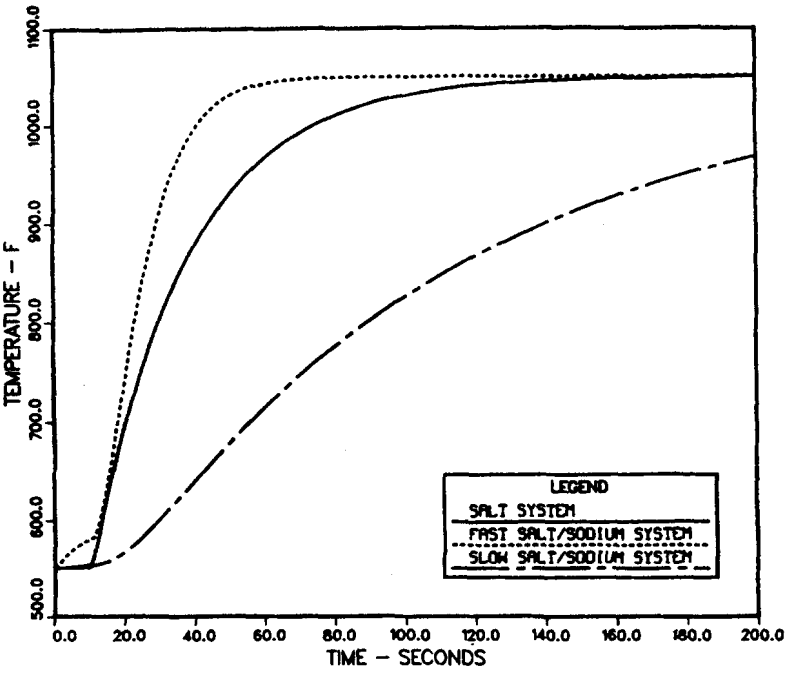

Figure ES-2. Comparison of the Delivered Molten Salt Temperatures for the Molten Salt and Liquid Sodium/Molten Salt Systems.

The annual energy used in this report is calculated from the the design point thermal power from the receiver less the thermal power equivalent of the electric power used to run the major system pumps. Since tower heights differ between north and surround fields, the required pumping power to flow the molten salt heat transfer fluid through the receiver will vary. The sodium systems have a closed sodium heat transfer loop which can be operated at the hydrostatic head. Therefore, the sodium receiver circulation pump has only to overcome the frictional parasitic drop. However, sodium system parasitics must include the molten salt circulation pump power consumption for cooling the sodium-to-salt heat exchanger.

It was thought that the parasitic pumping power requirements could be a deciding factor between system levelized energy costs. The greatest parasitic pumping power estimate was about 23 MW_t and the least about 10 MW_t. This results in a 2% effect, at best, on levelized energy cost. Therefore, the parasitic pumping power requirements are not a factor at the plant size considered in this report. Trace heating parasitics are not included since it was assumed there is no significant difference in the trace heating load required by each configuration.

The plant capital cost is calculated from cost models developed at SNLL based on Solar One data and cost estimates from reports[4,5,6]. Since many items do not vary in design from system to system, the major portion of the capital cost

is fixed. The important costs that vary between systems such as the receiver cost, tower cost, and pump costs are individually calculated for each case.

The levelized energy costs (LEC) for twelve system design cases were generated. The objective in this cost exercise was to calculate numbers that reflected the relative costs of the various system components so that comparisons may be made. Since the absolute value of the levelized energy cost can be misleading, only the levelized energy costs normalized to the greatest levelized energy cost are reported. The key system design characteristics and normalized LEC for each case are presented in Table ES-I. The normalized LEC as a function of peak flux is plotted in Figure ES-3.

Table ES-I. System Levelized Energy Cost

Case No.	Receiver Configuration	Peak Flux MW_t/m^2	Receiver Power MW_t	Receiver Area m^2	Tower Height m	Normalized LEC
1	external molten salt	0.24	480	3563	157	0.890
2	external molten salt	0.70	520	1539	179	0.767
3	external molten salt	1.78	522	679	183	0.739
4	external liquid sodium	0.24	480	3563	157	0.874
5	external liquid sodium	0.70	520	1539	179	0.767
6	external liquid sodium	1.78	522	679	183	0.745
7	cavity molten salt	0.24	548	7477	346	1.000
8	cavity molten salt	0.62	593	2406	352	0.774
9	cavity molten salt	1.82	565	681	353	0.755
10	cavity liquid sodium	0.24	550	7477	351	0.937
11	cavity liquid sodium	0.62	593	2406	352	0.755
12	cavity liquid sodium	1.82	565	681	353	0.752

In Table ES-I, external receivers are always matched to surround fields and cavity receivers are always matched to north fields. The receiver power is the power at the base of the receiver and varies from design to design because of varying receiver and field efficiencies. The tower height is the height of the tower from the ground to the base of the receiver.

Figure ES-3 shows that the levelized energy costs for all system configurations become essentially the same at peak flux levels above 0.7 MW_t/m^2. However, below 0.7 MW_t/m^2 the systems separate in levelized energy cost. The peak flux limits as determined in the Receiver Flux Limits section are marked on Figure ES-3. The corresponding normalized LEC's for a molten salt cavity receiver and external liquid sodium receiver are 0.88 and 0.75 respectively. This means the surround field/liquid sodium receiver configuration delivers energy that is 14% less expensive than the north field/molten salt cavity receiver configuration.

Due to the short period of time (2 months) available for preparing this report to meet internal deadlines, and the fact that information arrived from many sources at different times, it was not possible to obtain cost estimates for the systems at the nominal molten salt and liquid sodium peak flux levels of 0.46 and 1.02 MW_t/m^2 as determined in the System Efficiencies chapter. However, this does not prevent making comparisons that illustrate the factors affecting system levelized energy cost. Table ES-II presents a breakdown of the variable costs for

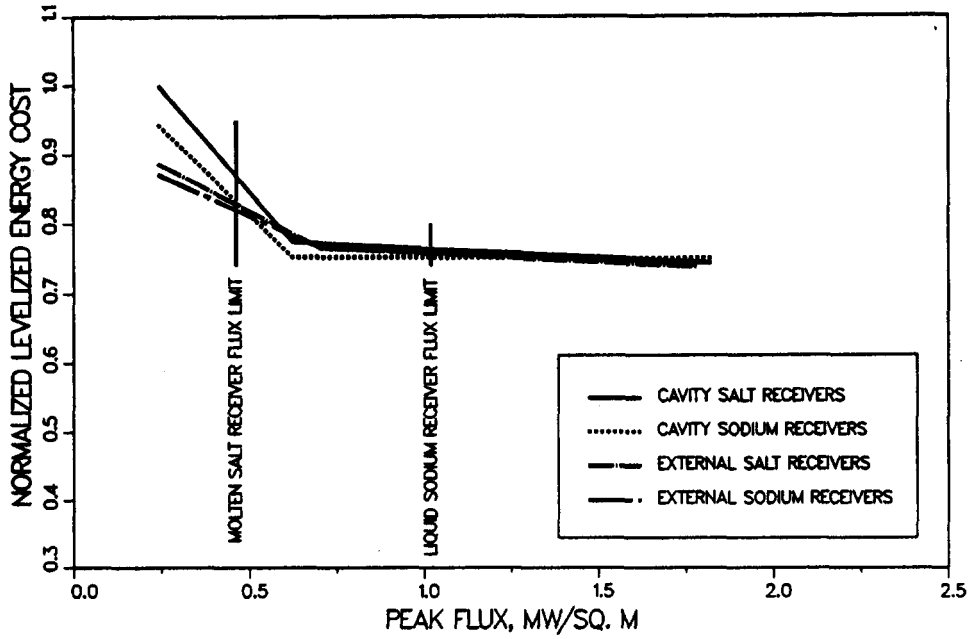

Figure ES-3. Economic Comparison of Heliostat Field/Receiver Combinations

four cases which are used to represent systems at molten salt peak flux levels and liquid sodium peak flux levels.

The major cost differences between a surround field/external liquid sodium receiver system and a north field/molten salt cavity receiver system are the absorber panel cost and the tower cost. The molten salt cavity receiver absorber cost is high because considerably more absorber area is required due to the reduced flux level, and because a more expensive tube material, Incoloy 800, is used. The tower cost is higher for a north field configuration than a surround field because a higher tower is required in order to achieve a reasonable system efficiency. The cost of the cavity structure and sodium-to-salt heat exchanger seem to be of secondary concern. The remaining items have a negligible effect.

The cost of the sodium-to-salt heat exchanger is particularly uncertain since it is unknown how one would be constructed. The primary cause of this uncertainty is that the reaction between sodium and molten nitrate salts at high temperature has not been studied experimentally. However, thermochemical calculations show that molten nitrate salts should react exothermically with liquid sodium[7]. Therefore, the cost of a sodium-to-salt heat exchanger could be much greater than the $7 million listed in Table ES-II. A sensitivity study shows that if the cost of the sodium-to-salt heat exchanger were to rise by $70 million, the cost advantage of a sodium/salt system would disappear. Since this capital cost difference is within the probable level of relative uncertainty of the system cost estimates (+/- 25%), it is entirely possible that cost uncertainties associated with

Table ES-II. Variable Cost Breakdown
(all costs are in millions of dollars)

Receiver Configuration	External		Cavity	
Receiver Fluid	Salt	Sodium	Salt	Sodium
Peak Flux	0.62	1.78	0.62	1.78
Receiver				
Absorber	14.3	3.4	22.3	3.5
Insulation	0.8	0.5	1.0	0.5
Shipping	0.3	0.1	0.4	0.1
Surge Tanks	3.0	3.4	3.3	3.6
Erection	11.2	5.0	17.5	5.0
Cavity Structure	0.0	0.0	7.6	2.2
Tower	6.0	5.9	42.2	42.7
Heat Transport				
Sodium-to-Salt HX	0.0	7.0	0.0	7.2
Sodium Handling Equipment	0.0	0.5	0.0	0.5
Sodium Argon Gas System	0.0	0.2	0.0	0.2
Sodium Valves	0.0	0.2	0.0	0.2
Molten Salt Receiver Pump	1.0	0.0	1.4	0.0
Molten Salt HX Circ. Pump	0.0	0.9	0.0	1.0
Capital Cost*	427.8	417.7	502.1	467.2

*not a sum of the above numbers

the sodium-to-salt heat exchanger could affect the cost advantage of the surround field/liquid sodium external receiver configuration.

Conclusions

The major conclusions are:

1. Generic north heliostat field/cavity receiver configurations are 6 to 10 percent more efficient than a generic surround field/external receiver configuration. This is due mostly to the better cosine efficiency of a north field.
2. There is little difference in the transient performance of a molten salt receiver compared to a sodium receiver connected to a sodium-to-salt heat exchanger. This is largely because the system time constants are controlled by the heat transfer capability and thermal inertia of the molten salt.
3. The surround field/liquid sodium external receiver configuration may provide energy at a 14 percent lower levelized energy cost than a north field/molten salt cavity receiver configuration. In spite of the efficiency advantage inherent in the north field/cavity receiver configuration, the higher capital cost of absorber and tower act to increase its levelized energy cost to above that of

a surround field/external receiver configuration. However, the cost advantage of the surround field/liquid sodium external receiver is not conclusive because of uncertainties in system components, notably the sodium-to-salt heat exchanger.

Recommendations

Based on the results of this study,

1. It is recommended that the surround field/liquid sodium external receiver configuration be considered as the reference configuration which will serve as a basis of comparison in future, more detailed studies.
2. It is recommended that more effort be placed on the improvement of cavity receiver design and performance estimates than on external receiver design and performance.
3. It is recommended that investigations into the design, construction and operation of a sodium-to-salt heat exchanger continue.

AN EVALUATION OF HELIOSTAT FIELD/RECEIVER CONFIGURATIONS

Introduction

It has been proposed by members of the solar community that a mid-size central receiver system of 35 to 80 MW_t utilizing a heat transfer fluid of either molten salt or liquid sodium be constructed and tested. The rationale is that a system of this size will reduce the uncertainties associated with solar thermal central receiver design and construction while costing far less than that required to construct and test a utility scale plant rated at 500 to 600 MW_t. However, it is anticipated that only one mid-sized plant will be constructed. Therefore, it is necessary to examine the current state of solar central receiver technology in order to determine which of the many potential concepts is most able to meet the needs of the users in the near future. This report presents a preliminary examination of the liquid sodium and molten nitrate salt solar central receiver technology.

Background

Solar thermal central receivers are characterized by a field of individual mirrors tracking the sun such that their combined reflections are concentrated on a receiver placed on top of a tower. The receiver serves as a heat exchanger transferring the concentrated radiant energy from the field of mirrors into a heat transport fluid. The configuration of the field of mirrors, called heliostats, and the tower can take two basic forms: a surround field and a north field.

The north field configuration as shown in Figure 1 is where all heliostats reside to the north of the receiver tower. Since northern heliostats have a better view of the sun, the north field configuration has a greater optical efficiency than the surround field configuration at low plant design power levels. As greater and greater power levels are sought, heliostats are added to the north until atmospheric attenuation reduces the radiant energy delivered to the receiver to below that delivered by heliostats in the south. At this point, heliostats are placed in the south in what is called the surround field configuration shown in Figure 2.

The selection of a north field or surround field configuration has a great impact on receiver design. There are two basic types of receiver designs: external and cavity. The external design, Figure 3, has the heat exchange surface exposed to the environment. There is no weather protection or obstruction to radiant energy delivered from the heliostat field. The cavity design, Figure 4, has the heat exchange surface enclosed in a protective structure or cavity. Radiant energy

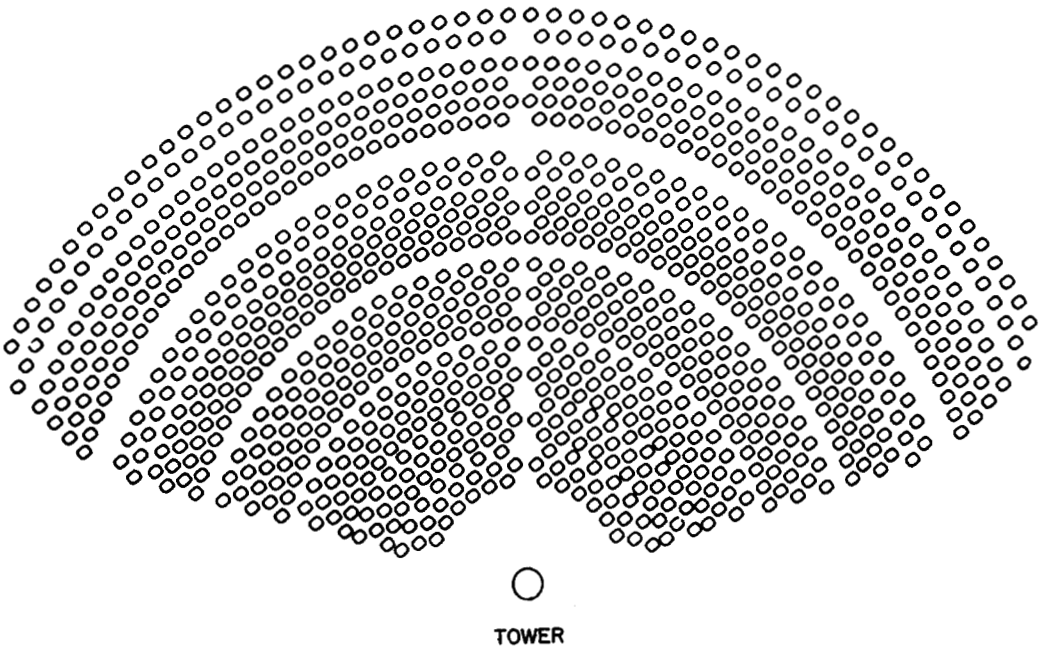

Figure 1. North Heliostat Field

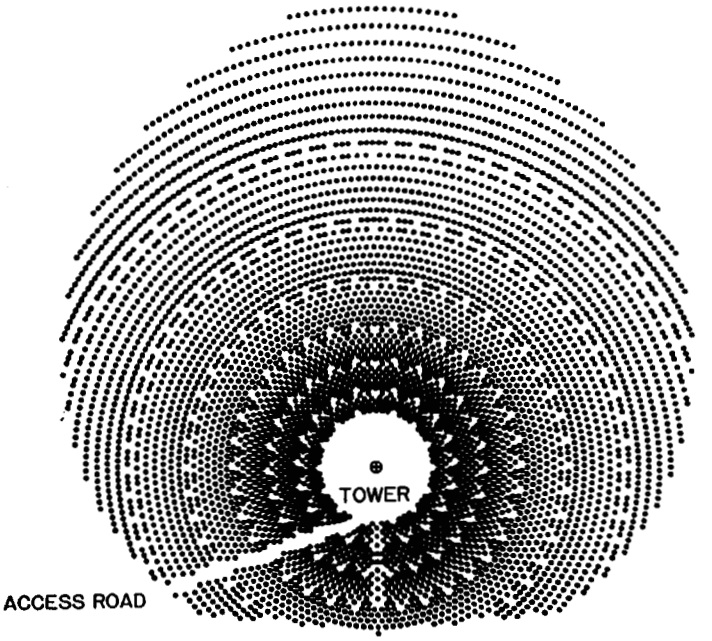

Figure 2. Surround Heliostat Field

from the heliostat field must pass through an aperture in order to strike the heat exchange surface.

External receiver designs may be cylindrical as shown in Figure 4, partial cylinders, or flat plates. Cavity receivers may have one or more cavities. The combination of receiver field configuration are as follows:

North Field

Flat Plate Receiver
Partial Cylinder Receiver
Single Cavity Receiver
Dual Cavity Receiver

Surround Field

Cylindrical Receiver
Quad or Four Cavity Receiver

Historically, the choice of a receiver fluid and power level has determined the receiver design and the field configuration. In this report, a heliostat field of 1,000,000 square meters of reflective area is selected as representative of future solar central receiver designs. This field size will deliver between 600 to 670 MW_t to a receiver depending on the field configuration, which leaves the receiver fluid selection as the major choice.

There are two leading candidates for central receiver systems: molten nitrate salt and liquid sodium. Liquid sodium and molten nitrate salt have quite different heat transfer rates. Nominally, liquid sodium has a heat transfer coefficient of around 40,000 W/m^2-$^\circ$C and molten salt around 8,500 W/m^2-$^\circ$C. This is a ratio of 4.7:1. By this simple comparison, sodium is the preferred choice as a receiver heat transfer fluid because of its greater cooling ability. Sodium receiver designs rated at around 500 MW_t are typically external cylinder designs with surround fields. The additional cost of a cavity structure was found to be excessive for the increase in receiver efficiency.

The choice between receiver fluids becomes complicated when thermal storage is added to the plant. Thermal storage is required to increase the overall plant capacity factor and capacity credit and increases operating flexibility. Adding thermal storage may also lower the levelized cost of energy delivered by the solar plant. Not surprisingly, liquid sodium and molten salt have quite different heat densities. The heat density of liquid sodium is around 0.336 $MWhr_t/m^3$-$^\circ$C and that of molten salt around 0.786 $MWhr_t/m^3$-$^\circ$C. This is a ratio of 1:2.3. Furthermore, the cost of storage is a consideration since the quantities of sodium or salt may become substantial if a high capacity factor is sought. Sodium sells for

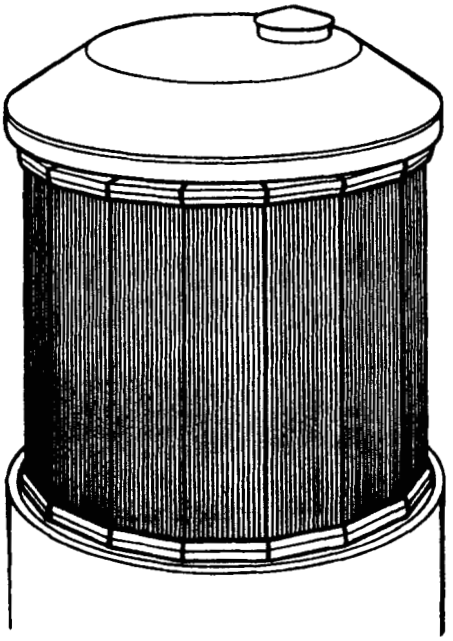

Figure 3. External Cylindrical Receiver

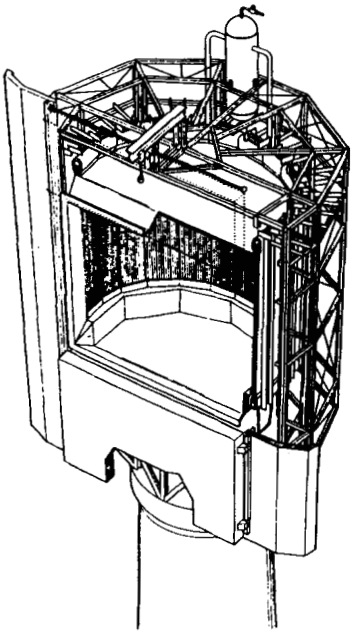

Figure 4. Single Cavity Receiver

around $1.76/kg installed compared to $0.84/kg installed for salt. This is a ratio of 2.1:1. By this simple comparison, molten salt is the preferred choice as a thermal storage medium.

The simplest solar thermal central receiver design is one where the receiver coolant is also the thermal storage medium. It was determined in 1980[8] that the sodium receiver with sodium storage is cost competitive with the salt receiver with salt storage only at low amounts of storage; in the range of 1 to 2 hours at rated receiver output. For capacity factors of 0.6, the storage capacities required are around 9 to 12 hours. Therefore, a high capacity factor plant would have a molten salt receiver and molten salt storage. The concept of coupling a sodium receiver with molten salt storage was postulated and examined in 1979[9]. The conclusion was that the cost of a sodium-to-salt heat exchanger was prohibitively high.

Since molten salt has a poorer heat transfer rate than liquid sodium, it must have more receiver area for the same thermal power rating. The increased receiver area increases the receiver thermal losses sufficiently for a cavity structure to pay for itself in increased receiver performance[3]. Therefore, molten salt receiver designs are typically cavity receivers.

Therefore, in 1980, the solar thermal central receiver plant configuration that had the best overall design value was a molten salt receiver with four cavities, one in each compass direction, a surround field, and molten salt storage. In the years since then, information has become available that has changed this configuration.

Since 1980, activity has concentrated on molten salt receiver designs. More detailed receiver designs[10,11] revealed difficulties with two sided heating of the tubes and the structural design. These revelations led to the eventual choice of a single cavity design with a north field configuration for molten salt systems. Costs developed for the more detailed molten salt receiver designs were much higher than anticipated in the 1980 comparison study. At the same time, the cost of heliostats decreased substantially making the receiver cost a greater portion of the overall plant cost. As a result, sodium receivers with their smaller size and anticipated lower cost, are once again under consideration.

In the current state of solar thermal receiver technology, there are four leading designs:

- Molten salt single cavity receiver, molten salt storage, north field.
- Molten salt external cylinder receiver with molten salt storage.
- Liquid sodium cavity receiver, molten salt storage, north field.
- Sodium external cylinder receiver with sodium-to-salt heat exchanger, molten salt storage, surround field. Sodium external receivers are predicted to cost less than molten salt cavity receivers because they have a smaller size and because they do not require an expensive cavity structure to have good thermal

performance. This economy would allow a sodium receiver with molten salt storage combination to achieve a lower levelized energy cost than a molten salt system.

Figure 5 is a schematic of the molten nitrate salt system. Molten salt from thermal storage at 288 ° C (550 ° F) flows into the receiver and exits at 566 ° C (1050 ° F). Figure 6 is a schematic of the sodium receiver/molten salt storage system. Molten salt from thermal storage at 288 ° C flows into the salt-to-sodium heat exchanger and exits at 566 ° C. The inlet and outlet temperatures of the sodium receiver are 28 ° C (50 ° F) hotter than those of the molten salt receiver. This temperature difference was chosen to provide adequate heat transfer, but may not be optimal.

Evaluation Methodology

This evaluation was conducted over a two month period in order to meet internal deadlines. Therefore, the evaluation is limited in scope and covers three main issues:

1. System efficiency - the overall efficiency of the heliostat field/receiver combination steady state will be determined. The system efficiency is defined as the product of the annual field efficiency and the design point receiver efficiency.

2. Transient performance - the startup time of each system will be determined.

3. Cost - the key system cost differences will be determined.

The first two issues allow the ability of each system to collect and absorb solar energy to be assessed. The last issue allows cost considerations to be included. The fundamental selection criterion is levelized energy cost. Additional factors are discussed in the Discussion chapter. Since receivers are designed to a particular flux constraint based on the working fluid, system designs are discriminated from each other by the receiver peak flux capability and heat transport fluid.

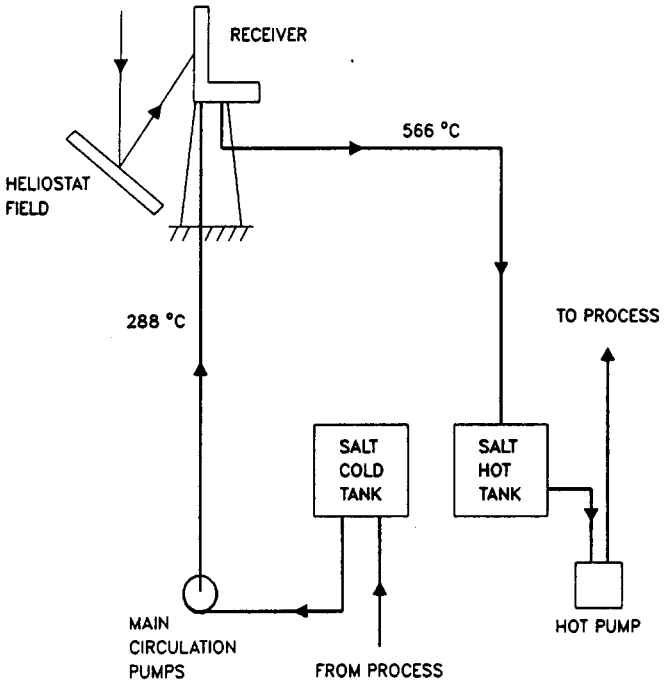

Figure 5. Molten Salt Receiver with Molten Salt Storage

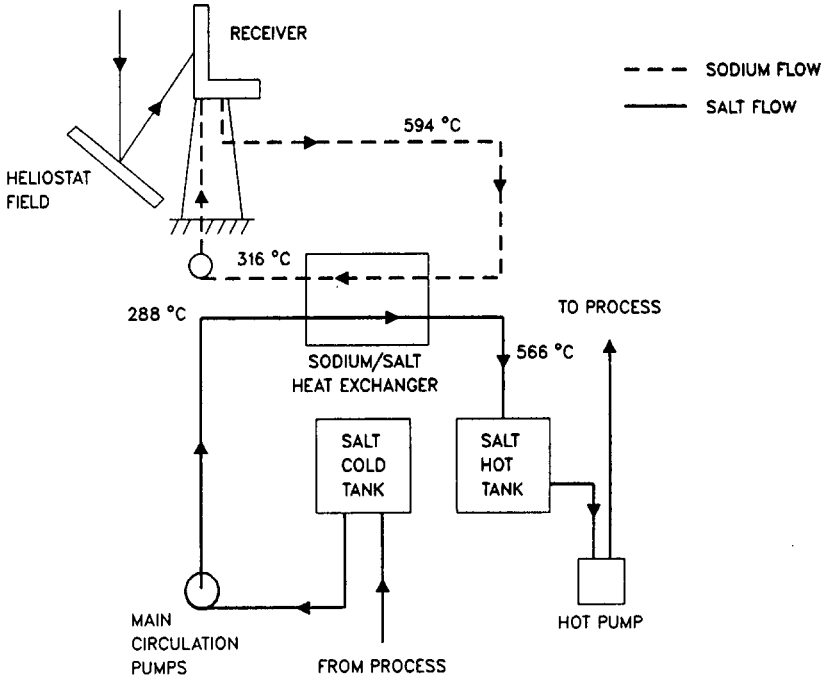

Figure 6. Liquid Sodium Receiver with Molten Salt Storage

System Efficiency

The conversion efficiency of solar energy to thermal energy controls the annual energy output of a solar thermal central receiver power plant. The greater the system efficiency, the more energy is captured for a given capital investment yielding a lower delivered energy cost.

Methodology

The system efficiency of cavity receivers was derived from the De Laquil and Anderson study on the performance of high temperature solar central receivers[1]. The system efficiency of external receivers was derived in a similar manner so the system efficiencies could be compared. The computer code, DELSOL2[2], developed at Sandia National Laboratories - Livermore (SNLL), was used for the heliostat field design and receiver design except where noted. The key heliostat field design assumptions are:

1. Field size fixed at 1,000,000 m^2.
2. All heliostats canted and focussed at their slant range.
3. Heliostat size fixed at 50 m^2.
4. Heliostat configuration is DELSOL2 default heliostat with 12 cant panels in a 2 wide by 6 high array.
5. Heliostat reflectivity fixed at 0.89.
6. Design point is noon on day 81 (vernal equinox).
7. Design insolation is 950 W/m^2.

The heliostats were focussed and canted at their slant range for all field designs considered in this report. This option creates the smallest heliostat beam size possible which reduces spillage losses and the aperture size for cavity receivers and the diameter of external receivers. However, it is not economical to manufacture such customized heliostats. A more typical installation would have one or two different slant ranges at which the heliostats are focussed and canted. De Laquil and Anderson demonstrated that the loss in north field efficiency when using a single slant range is minimal. The same effect is assumed for surround fields.

Cavity receiver geometry was determined by De Laquil and Anderson using DELSOL2. Cavity receiver performance was calculated by De Laquil and Anderson external to the DELSOL2 optimization routines using programs RADSOLVER[12] and SHAPEFACTOR[13] for the radiative heat transfer, and a correlation by J. Kraabel[14] for the natural convection losses. Forced convection

losses were not calculated. Reference 1 contains a discussion of the cavity receiver performance calculations.

The cavity receiver losses calculated by De Laquil and Anderson were for advanced high temperature receivers with average receiver absorber surface temperatures of 600 ° C to 2100 ° C. A more representative average absorber surface temperature for current receivers is 480 ° C. The De Laquil and Anderson receiver performance results for a 600 ° C receiver are scaled to 480 ° C for use in this report. The convective losses are scaled by holding the absorber area constant and reducing the average absorber surface temperature. The radiative losses are scaled varying both the absorber surface temperature and the aperture area. The scaling equations used are:

Convective Losses

$$C_{480} = \frac{(753 - 293)^{1.43}}{(893 - 293)^{1.43}} C_{600}$$

Radiative Losses

$$R_{480} = \frac{AA_{480}(753^4 - 293^4)}{AA_{600}(873^4 - 293^4)} R_{600}$$

where,

AA_{480} = the cavity aperture area at 480 ° C
AA_{600} = the cavity aperture area at 600 ° C
C_{480} = convective losses at 480 ° C
C_{600} = convective losses at 600 ° C
R_{480} = radiative losses at 480 ° C
R_{600} = radiative losses at 600 ° C

The external receiver height and width are determined by DELSOL2. The external receiver performance is calculated using the convective loss correlations suggested by D. Siebers[14] and the Stefan-Boltzman law of radiation:

Natural Convection

$$Nu_N = 0.098 Gr_H^{1/3} \left(\frac{T_w}{T_a}\right)^{-0.14}$$

Forced Convection

$$Nu_F = 1.36\text{x}10^{-3} Re_D^{0.98} + 6.345\text{x}10^{-3} Re_D^{0.89}$$

Combined Convection

$$h_{mixed} = \left[\left(\frac{Nu_N k_a}{H} \right)^{3.2} + \left(\frac{Nu_F k_f}{D} \right)^{3.2} \right]^{1/3.2}$$

$$Q_{loss_{conv}} = h_{mixed}(\pi DH)(T_w - T_a)$$

Radiation

$$Q_{loss_{rad}} = \epsilon\sigma(\pi DH)(T_w^4 - T_a^4)$$

Total Receiver Thermal Losses

$$Q_{tot} = Q_{loss_{conv}} + Q_{loss_{rad}}$$

where,

D = receiver diameter
Gr_H = Grashof number based on the receiver height (fluid properties calculated at the ambient temperature)
H = receiver height
h_{mixed} = combined heat transfer coefficient for natural and forced convection
k_a = air thermal conductivity at ambient temperature
k_f = air thermal conductivity at the film temperature
Nu_N = Nusselt number for natural convection
Nu_F = Nusselt number for forced convection
Re_D = Reynolds number based on the receiver diameter (fluid properties calculated at the film temperature, air velocity of 4.5 m/s (10 mph) assumed)
T_w = average receiver surface temperature, K
T_a = ambient temperature, K
ϵ = receiver emissivity = 0.93
T_f = film temperature = $(T_f + T_w)/2$

The above relations were implemented in DELSOL2 in place of the existing algorithm providing more realistic estimates of the radiative and convective losses during the optimization process. An average receiver surface temperature of 480 ° C is used as representative of all molten salt and sodium receivers.

Results

The system efficiency as a function of peak flux is shown in Figure 7. The system efficiency is defined as the product of the annual field efficiency and the

design point receiver efficiency. This definition of the system efficiency was used by De Laquil and Anderson and is continued in this report. The effect of this definition is to overstate the system efficiency since any reduction in receiver efficiency at part load is not included. It is assumed that all receivers are similarly affected by part load operation. Therefore, while the system efficiencies quoted here are not necessarily accurate on an absolute basis, they are sufficient for a relative comparison.

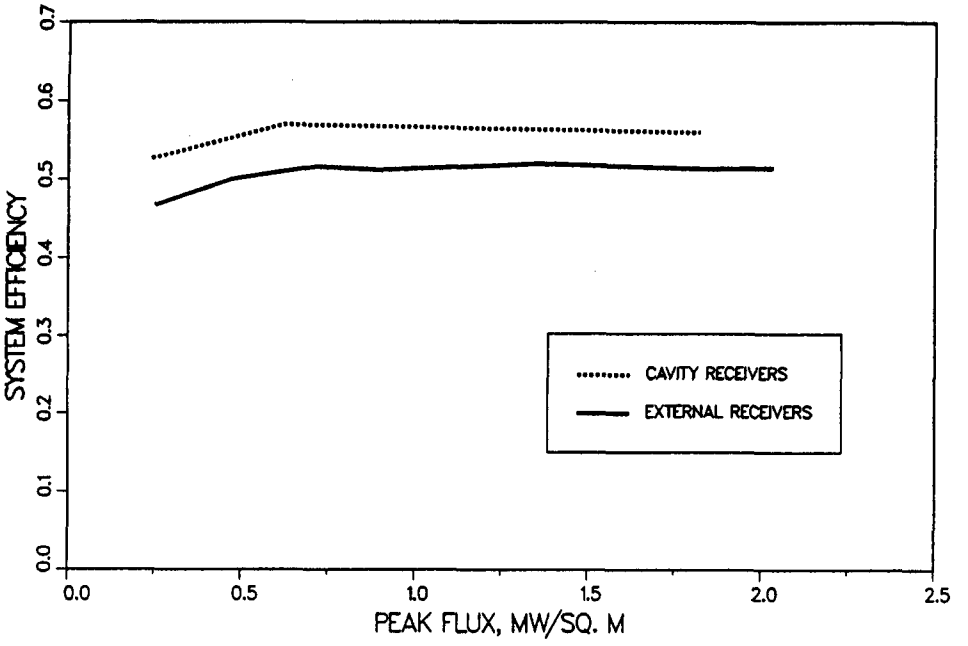

Figure 7. System Efficiencies

The most significant observation to be made from Figure 7 is that the cavity receiver/north field systems are about 10% more efficient than the external receiver/surround field systems. This is due almost entirely to the difference in the cosine efficiency of the two fields. This difference agrees well with that presented in a report published in 1979 by the Martin-Marietta Corporation (MMC)[3]. In this report, MMC calculated that a north field would deliver 9.3% more energy in a year than a surround field with the same number of heliostats based solely on the differences in their cosine efficiency. When all effects are included, such as shadowing and blocking, the difference in heliostat field efficiency can account for around 7 percentage points of the difference in system efficiency.

The cosine efficiency of the north field is not explicitly stated by De Laquil and Anderson, but can be back-calculated using general factors for reflectivity, shadowing, blocking, and atmospheric attenuation for a north field. These are 0.89, 0.99, 0.98, and 0.92 respectively. Applying these factors to the field efficiency of 0.64 quoted by De Laquil and Anderson, the annual north field cosine is found to be approximately 0.82. Table I contrasts these north field parameters

Table I. Field Performance Parameters

	North Field	Surround Field
Reflectivity	0.89	0.89
Shadowing	0.99	0.98
Cosine	0.82	0.75
Blocking	0.98	0.99
Atmospheric Attenuation	0.90	0.92
Total Field Efficiency	0.64	0.60

with those typically calculated by DELSOL2 for the surround fields designed for this report.

The receiver design point efficiency, which is required to complete the system efficiency calculation, is determined from receiver loss fractions for spillage, radiation, and convection. The receiver loss fraction is defined as the thermal power lost due to a particular loss divided by the available thermal power from the field. The receiver loss factors for three peak flux levels are shown in Table II for the cavity and external receivers designed for this report. The design point for all receivers is solar noon, on day 81 (spring equinox). The radiation loss includes reflected incident radiation as well as emitted radiation. The reader should be aware that the receiver loss factors are additive whereas the heliostat field performance parameters are multiplicative.

It can be seen from Table II that the cavity receivers have a greater efficiency than the external receivers until high peak flux levels are attained. This result is anticipated since the receiver radiative losses are greatly reduced when a cavity enclosure is used. It is interesting to note that the convective losses for the cavity receiver are greater than those for the external receiver until high peak flux levels are reached. Typically, it is thought that the cavity enclosure reduces convection losses compared to an external receiver. The discrepancy may be due to the convective loss correlation used, but is probably strongly influenced by the relationship between the average and peak flux for each type of receiver. This relationship will be discussed next.

Figures 8 and 9 illustrate how the average to peak flux ratio varies as a function of peak flux for a cavity and external receiver respectively. The average flux determines the active surface area of the receiver which in turn is a factor in calculating the convective heat loss. The two figures show that the rate of increase in receiver area decreases with decreasing peak flux for external receivers while the exact opposite effect occurs with the cavity receivers. Therefore, at low peak fluxes, cavity receivers have much more absorber area (more than 2 times at a peak flux of 0.24 MW_t/m^2) than external receivers designed to the same peak flux. It is not clear why this behavior exists. It may be a physical consequence inherent in the design, or it may be a consequence inherent in the design tools employed. Resolution of this matter is beyond the scope of this report.

Table II. Receiver Loss Factors

Peak Flux = 0.24 MW_t/m^2		
	Cavity Receiver	External Receiver
Spillage	0.04	0.005
Radiation	0.02	0.166
Convection	0.115	0.044
Total	0.175	0.214
Peak Flux = 0.62 MW_t/m^2		
	Cavity Receiver	External Receiver
Spillage	0.04	0.020
Radiation	0.036	0.110
Convection	0.029	0.019
Total	0.105	0.149
Peak Flux = 1.8 MW_t/m^2		
	Cavity Receiver	External Receiver
Spillage	0.06	0.04
Radiation	0.078	0.086
Convection	0.007	0.009
Total	0.145	0.135

The system efficiency is calculated by the following equation:

System Efficiency = Field Efficiency x (1 - Total Receiver Loss Fraction)

Table III contains the system efficiencies for the three peak flux levels and field/receiver combinations.

Receiver Flux Limits

The system efficiencies presented in the previous section were calculated without regard to the heat transfer fluid used to cool the receiver. The selection of a heat transfer fluid controls the maximum peak flux that a tube can endure which in turn determines the maximum system efficiency. In particular, it is the heat transfer coefficient of the fluid that controls the level of thermal fatigue the receiver tubes experience and the level of thermal fatigue controls the receiver lifetime. A linear analysis has been developed at SNLL which relates heat transfer coefficient, peak tube crown temperature, tube outside diameter, tube wall thickness, allowable strain range, and peak flux[15]. The allowable strain range is based on ASME code case 1542 (N47).

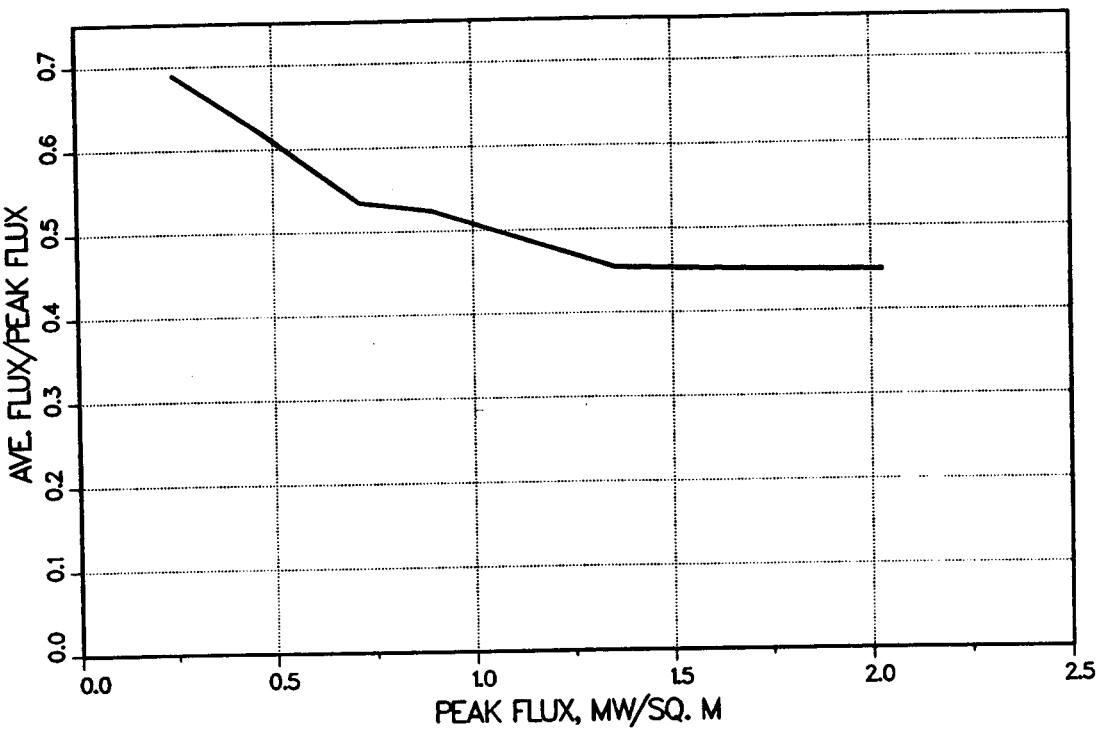

Figure 8. Flux Ratio for External Receivers

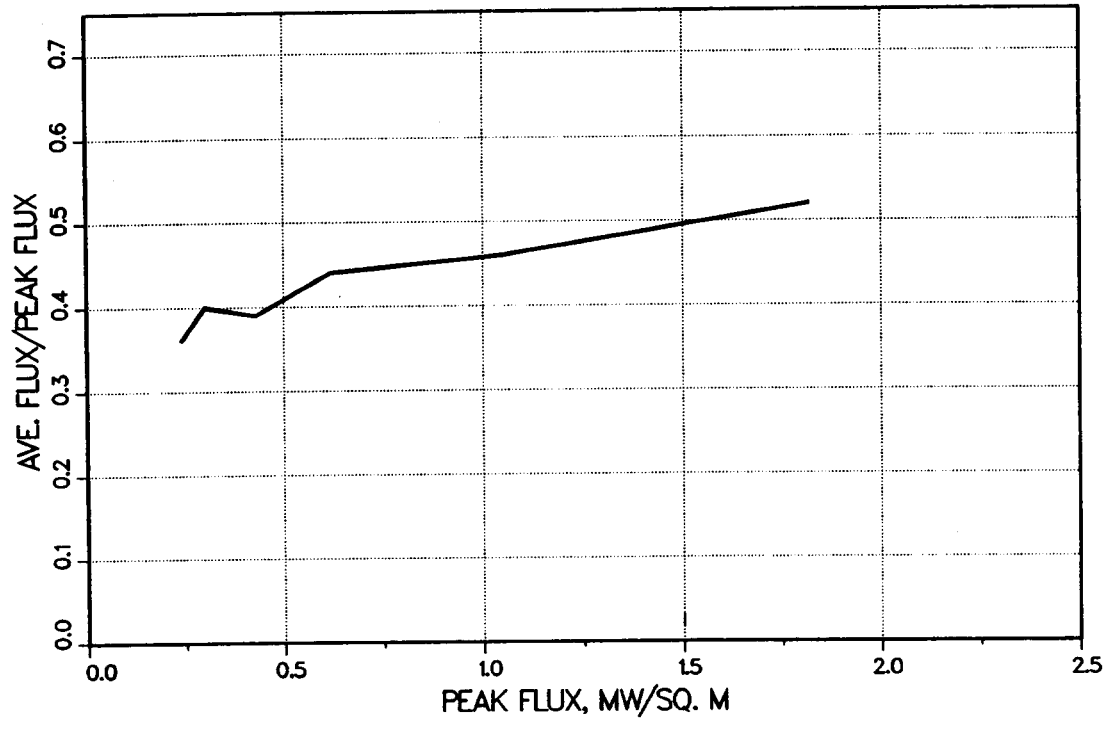

Figure 9. Flux Ratio for Cavity Receivers

Table III. System Efficiencies

Configuration	Peak Flux in MW_t/m^2 0.24	0.62	1.8
Cavity Receiver/North Field	0.53	0.57	0.55
External Receiver/Surround Field	0.47	0.51	0.52

Figures 10 and 11 are samples of the results that can be obtained from the linear model for a molten salt receiver and a liquid sodium receiver respectively. For the purposes of comparison, the set of parameter values listed in Table IV will be used throughout the remainder of this report. The details of designing a receiver will not be addressed in this report. The peak allowable fluxes for these parameter values are 1.02 MW_t/m^2 and 0.46 MW_t/m^2 for a liquid sodium receiver and molten salt receiver respectively.

Summary

The key results of this chapter are:

1. North heliostat fields are approximately 7% more efficient than surround fields of the same reflective area. The majority of this effect is due to differences in the field cosine efficiency.

2. Cavity receivers have, in general, better thermal efficiency than external receivers. This is largely due to the reduction in radiative losses when a cavity enclosure is employed.

3. Cavity receivers have, in general, greater convective losses than external receivers. This is because the cavity receivers have up to twice the absorber surface area of external receivers for the same peak flux.

4. A north field/cavity receiver system configuration is 6 to 10 percent more efficient than a surround field/external receiver system configuration.

5. The peak flux limit for a molten salt receiver is roughly half that of a sodium receiver, i.e., 0.46 MW_t/m^2 versus 1.02 MW_t $/m^2$ respectively.

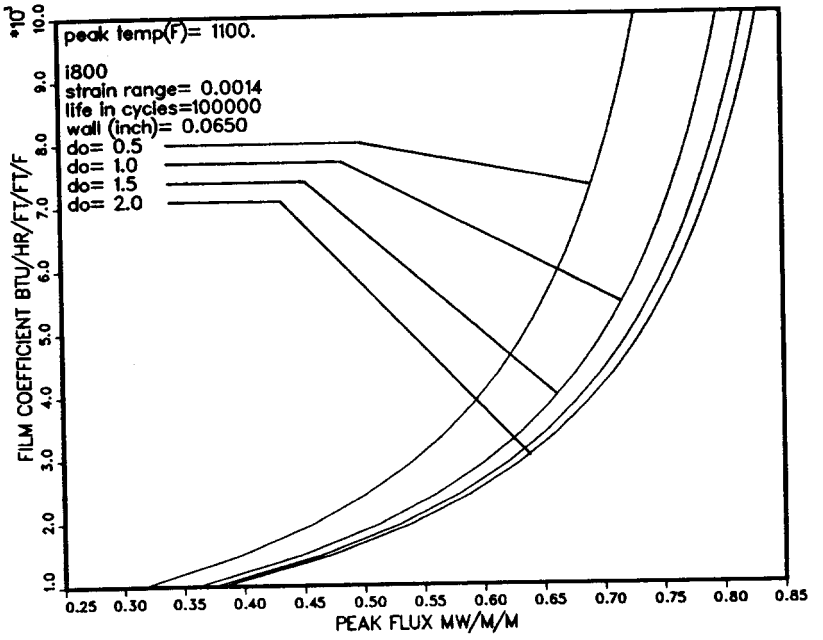

Figure 10. Allowable Peak Flux for a Molten Salt Cooled Tube at a Peak Temperature of 593 ° C

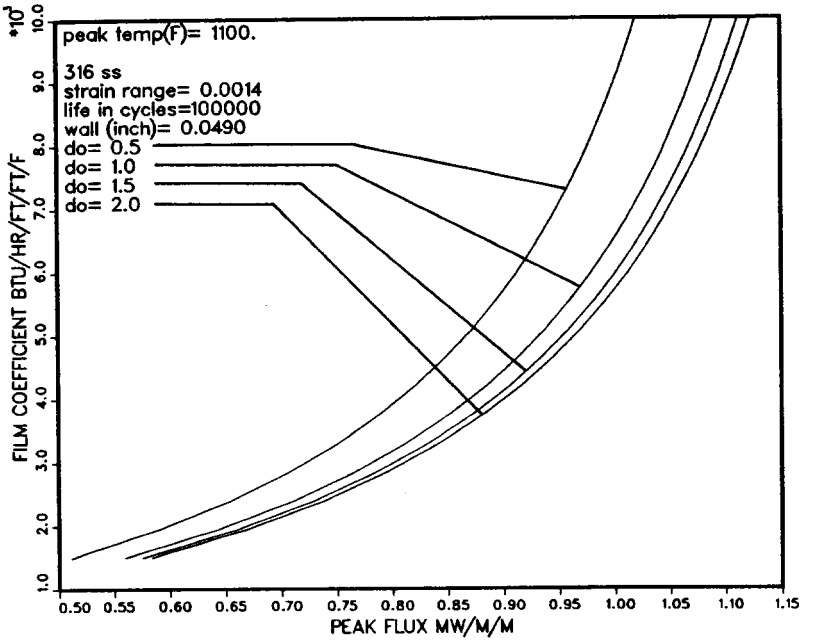

Figure 11. Allowable Peak Flux for a Liquid Sodium Cooled Tube at a Peak Temperature of 593 ° C

Table IV. Receiver Thermal/Mechanical Design Parameters

Tube outside diameter	2.54 cm (1.0 in.)
Tube wall thickness - molten salt	1.65 mm (0.065 in.)
liquid sodium	1.24 mm (0.049 in.)
Tube material - molten salt	Incoloy 800
liquid sodium	316 Stainless Steel
Heat transfer coefficient - molten salt	8,500 W/m^2-°C (1500 B/h-ft^2-°F)
Heat transfer coefficient - liquid sodium	40,000 W/m^2-°C (7,000 B/h-ft^2-°F)
Tube life	100,000 cycles
Peak tube temperature	593 °C (1100 °F)
Allowable stress range	from N47

Transient Performance

While the objective of the salt and salt/sodium system is to produce a steady flow of 566 ° C (1050 ° F) molten salt, the hardware configuration for the two systems suggests possible differences in the transient behavior, particularly at startup. This is reflected in the time required to produce steady state flow of 566 ° C salt in an initially cold system. For two systems producing hot molten salt at the same rate, one can expect the thermal mass of the sodium receiver to be substantially less (due primarily to higher flux levels) than for the salt receiver. Hence startup times for the sodium receiver should be significantly less than the salt receiver. However the sodium/salt system is handicapped at startup by the need to thermally condition (i.e., bring to steady state temperature) a potentially massive sodium-to-salt heat exchanger. This situation makes an assessment of startup times more difficult.

In this chapter, numerical models will be used to compare startup times for the salt and sodium/salt systems. It is emphasized that this study considers only the thermal inertia characteristics for the two systems. It is assumed that the rate of applying solar flux to each system is identical and that thermal conditioning of the heat exchanger occurs simultaneously with the receiver. Certain operational and/or safety considerations peculiar to one system are not addressed here, such as the need to apply flux more slowly to sodium tubes than to salt tubes (or vice versa). Furthermore, startup limitations in the receiver and heat exchanger control algorithms are not considered.

Appendix A describes the simplified lumped parameter models for the salt and salt/sodium systems. These models were used to perform parametric studies in order to determine relative startup time differences between the two systems for a variety of hardware designs and operating conditions. Results from the parametric studies are discussed in the remaining sections of this chapter.

Parametric Studies

Parameters for the base case salt and sodium receivers are summarized in Table V. The tube inside diameters and outside diameters were selected from actual receiver designs and reflect both the thermo-mechanical and corrosion requirements. The flux levels listed are considered typical for salt and sodium receivers. The mass flow rate for each receiver was selected so that the average fluid velocity in each tube was 2.4 m/s (8 ft/sec). This velocity gives rise to acceptable pressure drops for both receiver tubes including the lengthy salt receiver tube. With these parameters fixed, the steady state lumped parameter receiver equations can

Table V. Parameters for the Base Case Salt and Sodium Receivers

Parameter	Salt Receiver	Sodium Receiver
Average Flux (MW_t/m^2)	0.3	0.6
Tube ID (cm)	2.2	2.3
Tube OD (cm)	2.5	2.5
Tube Length (m)	94.0	20.0
Average Velocity (m/s)	2.4	2.4
Inlet Temperature (° C)	288.0	316.0
Outlet Temperature (° C)	566.0	594.0
$\dot{m}c$ (kW/ ° C)	2.584	1.094
Δp^* (kPa)	590.0	54.5

*Frictional pressure drop is based on the average fluid velocity, constant fluid properties, and a tube wall roughness (ϵ/D) of 0.0015

be solved to compute the required tube length for the desired outlet temperature. These lengths are also listed in Table V.

The calculated $\dot{m}c$ indicates that the absorbed power per receiver tube is 2.36 times greater for the salt receiver than for the sodium receiver when each fluid undergoes a 278 ° C (500 ° F) temperature change. Thus for receivers of identical total power level, the sodium receiver will have more than twice as many tubes as the salt receiver. Since the tubes are in parallel the number of tubes does not affect the startup time. Thus receiver startup times can be estimated through an analysis of a single receiver tube. Furthermore startup time comparisons between sodium and salt tubes having different power levels ($\dot{m}c$) are valid because all tubes possess the length required to absorb enough energy to produce the desired outlet temperature.

Since the flux level and tube geometry for the salt and sodium base case receivers are representative of actual designs, these parameters were not altered in the parametric study. The only remaining parameter which could vary between receiver designs is the average fluid velocity V_R, although large velocities would probably never be used since they lead to excessive pressure drops.

The influence of the average velocity appears to be negligible as demonstrated in Table VI which compares the step flux startup time constants for three salt receivers having different average fluid velocities. Although the tube length, pressure drop, and power level for each receiver tube varies with the average velocity, the startup times remain the same. A salt receiver with V_R = 4.8 m/s (16 ft/s) would not be an acceptable design because of the excessive frictional pressure drop resulting from increased tube length and fluid velocity ($\Delta P \sim LV_R^2$).

It appears that conclusions drawn from comparing the relative startup times of the base case salt and sodium receivers will be applicable to any "reasonably" designed salt or sodium receiver. The step flux startup time constants for the

Table VI. Influence of Average Fluid Velocity on the Design and Startup Time for Salt Receivers

Velocity m/s	Flow Length m	Δp kPa	$\dot{m}c$ kW/ ° C	t s
1.2	47.2	78.0	1.29	28.0
2.4	94.2	590.0	2.58	28.0
4.8	188.0	4560	5.17	28.0

base case salt and sodium receivers are 28.2 and 7.4 seconds respectively. From these times it is reasonable to conclude that based on heat capacity arguments alone, salt receivers are at most 3.8 times slower to start up than sodium receivers. This difference will be less if the flux is applied at a slower rate to each receiver.

Drawing general conclusions regarding the startup times required to produce 566 ° C salt in the salt and sodium/salt systems is considerably more difficult than drawing general conclusions for salt and sodium receivers. Unlike the receiver designs, the heat exchanger design in the sodium/salt system is not well defined.

In order to arrive at general conclusions regarding the salt and sodium/salt systems, a "base case" heat exchanger design will be proposed. The parameters and configuration for this base case heat exchanger are based on proposed designs for similar heat exchangers in solar application. A 100 % efficient counterflow heat exchanger (i.e., no heat loss through the shell) is assumed. Sodium flows in the tubes and salt flows on the shell-side.

The startup time for the entire heat exchanger was determined by calculating the startup time for a single representative sodium tube surrounded by an appropriate fraction of the total salt shell flow. The shell and tube masses on a per tube-per unit length basis are:

tube:

$$\frac{m}{L}_t = \frac{\textit{total heat exchanger tube mass}}{\textit{single tube length x number of tubes}}$$

shell:

$$\frac{m}{L}_s = \frac{\textit{total shell mass}}{\textit{single tube length x number of tubes}}$$

Other parameters required to establish the heat exchanger design are summarized in Table VII along with the base case numerical values. The first five parameters in the table, N_T, D_T, $(m/L)_t$, $(m/L)_s$, and V_S, completely specify the design. The remaining parameters may be calculated directly assuming annular geometry. It is also assumed that the entire flow from a single sodium receiver tube is divided into N_T tubes in the heat exchanger. With the steady state inlet

Table VII. Parameters for the Base Case Heat Exchanger Designs

Parameter	Symbol	Units	Value
Number of HX tubes per receiver tube	N_t	-	1
ID of the HX tube	D_t	cm	2.4
Tube mass parameter	$(m/L)_t$	kg/m	0.541
Shell mass parameter	$(m/L)_s$	kg/m	0.419
Average salt velocity	V_S	m/s	0.780
Average sodium velocity	V_N	m/s	2.30
Salt $\dot{m}c$	$(\dot{m}c)_S$	kw/ ° C	1.09
Sodium $\dot{m}c$	$(\dot{m}c)_N$	kw/ ° C	1.09
Salt pressure drop	Δp_S	kPa	77.2
Sodium pressure drop	Δp_N	kPa	95.9
Flow Length	L_{HX}	m	41.1

and outlet salt and sodium temperatures known, it is possible to solve directly for the heat exchanger length.

In the discussion which follows, the five design parameters for the heat exchanger are varied over reasonable ranges in order to determine their effect on the startup time of a sodium/salt system. In all cases, the base case sodium receiver parameters are used to specify the receiver design. A step flux is applied at t=10 seconds.

The influence of N_T is shown in Figure 12. The rise in salt temperature prior to the time when the solar flux is applied (i.e., t=10 seconds) is due to the flow of 316 ° C sodium into the initially uniform 288 ° C heat exchanger. This causes a slight increase in outlet salt temperature beginning at t=0. This rise is evident in all the sodium/salt response curves.

Figure 12 shows that increasing the number of heat exchanger tubes per receiver tube results in faster startup times for the sodium/salt system. This is primarily due to the fact that the lower flow rates brought about by dividing the receiver flow into two parallel heat exchanger flow paths permits the length (and hence heat capacity in a single flow path) of the heat exchanger to be reduced by approximately half.

The influence of the heat exchanger sodium tube inside diameter is illustrated in Figure 13. Larger tube inside diameters produce more rapid startup times. As the inside diameters are increased the heat transfer area between the salt and sodium is increased. This increase allows shorter flow paths with less heat capacity to be used, hence the faster startup times.

Figures 14 and 15 illustrate the influence of tube and shell mass parameters. In each case these parameters appear to have a negligible influence on the startup times.

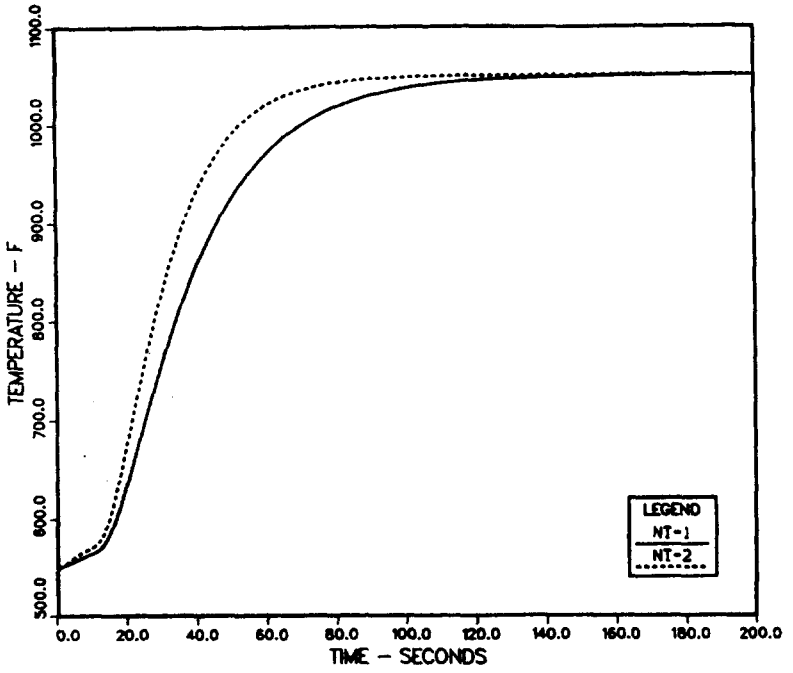

Figure 12. Comparison of Delivered Molten Salt Temperatures from the Liquid Sodium/Molten Salt System for Step Flux Change–Parameter: Number of Heat Exchanger Tubes per Receiver Tube

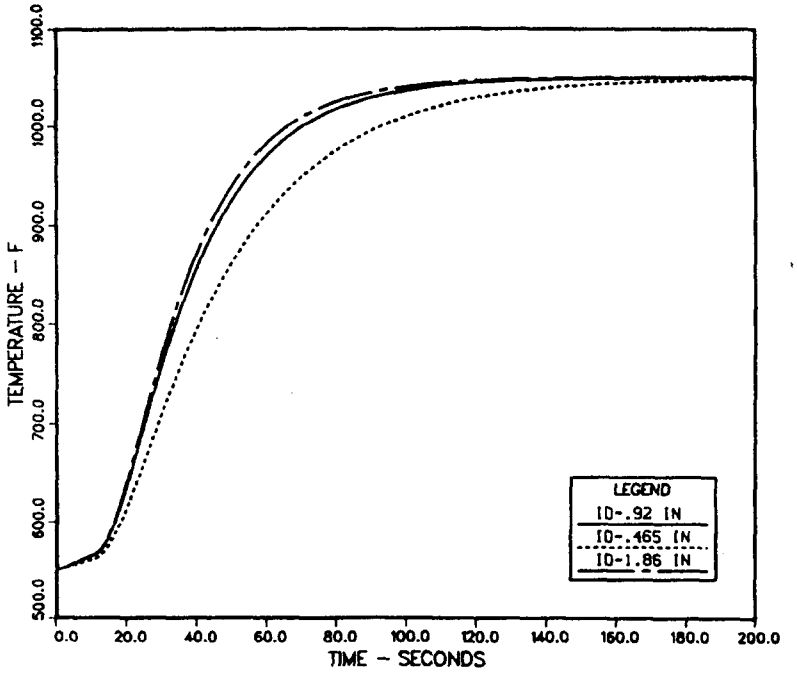

Figure 13. Comparison of Delivered Molten Salt Temperatures from Liquid Sodium/Molten Salt system for Step Flux Change–Parameter: Heat Exchanger Tube Inside Diameter

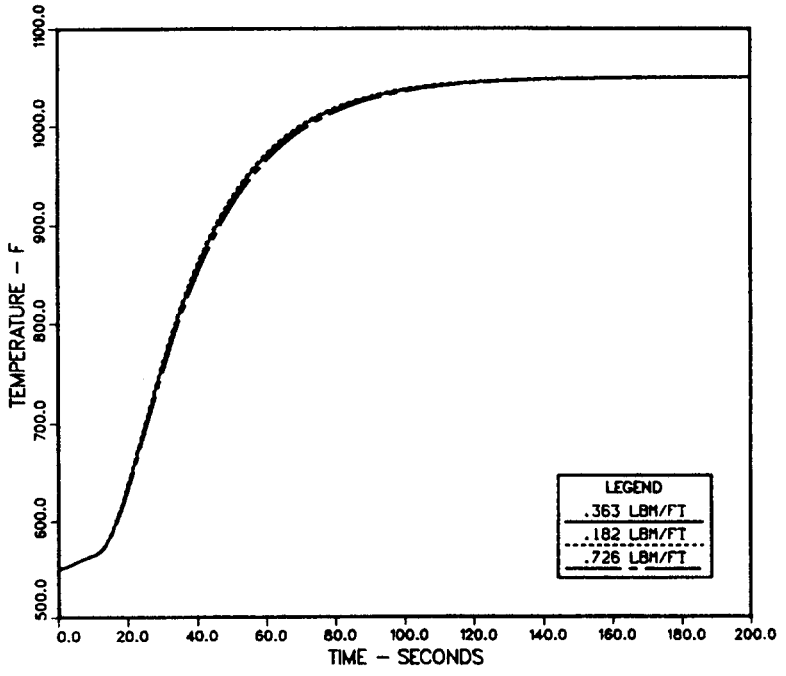

Figure 14. Comparison of Delivered Molten Salt Temperatures from Liquid Sodium/Molten Salt system for Step Flux Change–Parameter: Heat Exchanger Tube Mass per Unit Length

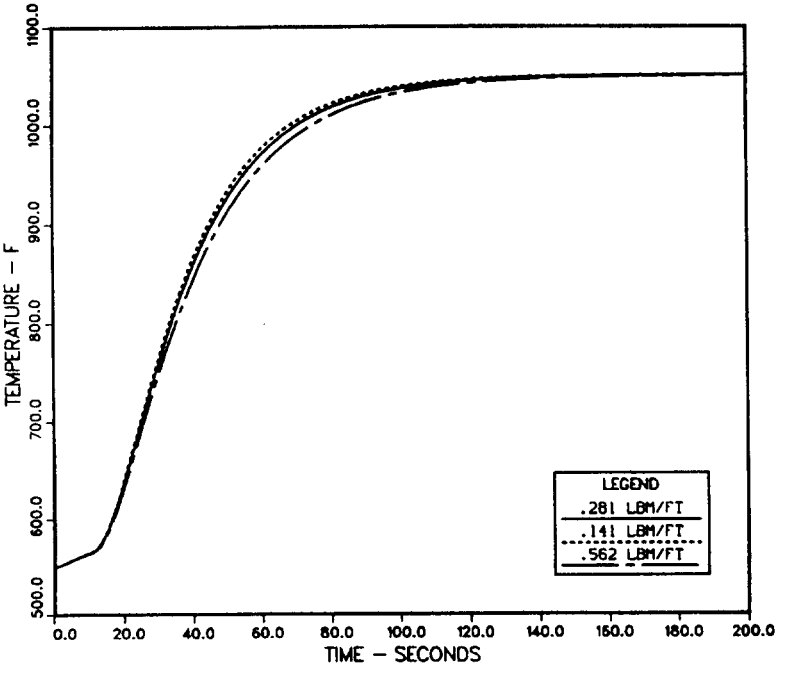

Figure 15. Comparison of Delivered Molten Salt Temperatures from Liquid Sodium/Molten Salt system for Step Flux Change–Parameter: Heat Exchanger Shell Mass per Unit Length

The influence of the final heat exchanger design parameter, V_S, is illustrated in Figure 16. Lower salt velocity results in substantially lower salt-side heat transfer coefficients. The salt-side heat transfer coefficient and area comprise the larger portion of the total heat exchanger conductance. Therefore, a longer heat exchanger flow path is required to provide 566 ° C salt at the outlet. The result is increased startup times.

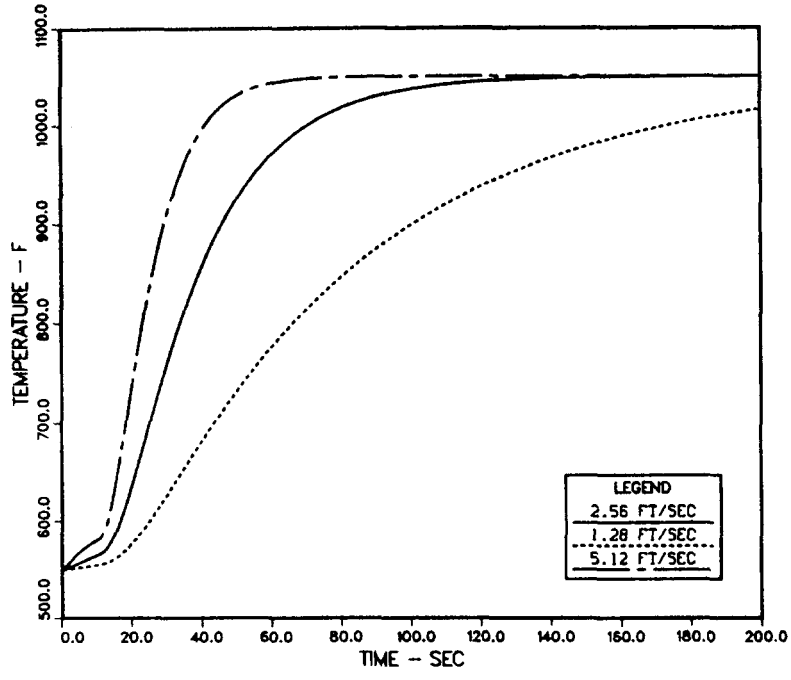

Figure 16. Comparison of Delivered Molten Salt Temperatures from Liquid Sodium/Molten Salt system for Step Flux Change–Parameter: Average Heat Exchanger Molten Salt Velocity

The study of relative startup times for the salt and sodium/salt systems begins with a comparison of the base case systems shown in Figure 17. For the base case comparisons, the step flux startup times are essentially equal. The more rapid response of the sodium receiver appears to be counterbalanced by the lag in the sodium/salt heat exchanger. Hence, when the two components are operated in series the overall time required to produce steady state 566 ° C salt is near that of the salt system.

The influence of simultaneously varying multiple heat exchanger design parameters on the startup time comparison is illustrated in Figure 18. Two heat exchanger designs are considered. The "fast" heat exchanger design is the design which results when the parameters which produced rapid startup are combined into one design. Similarly, the "slow" heat exchanger is the design resulting from combining parameters which produce slower responses.

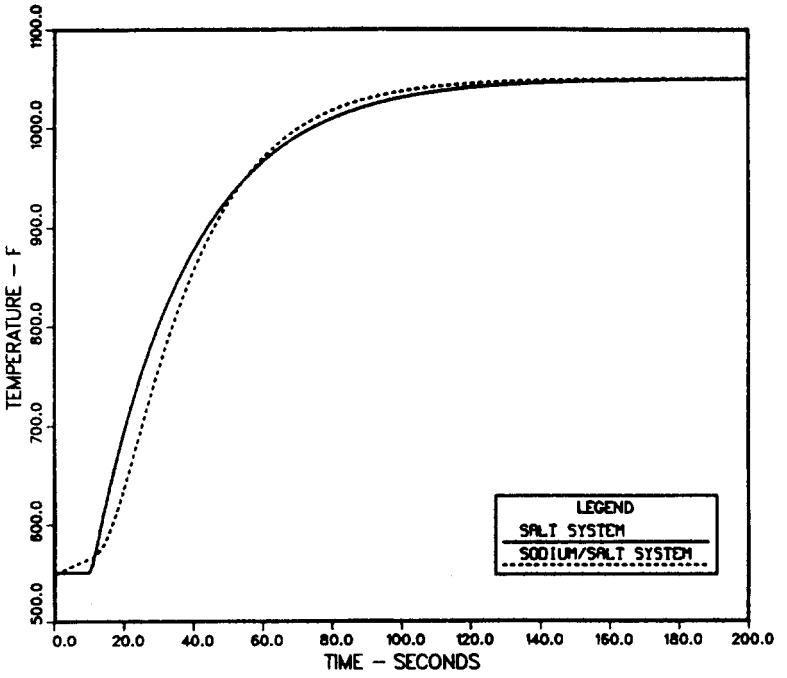

Figure 17. Temperature History for Delivered Molten Salt for the Molten Salt and Liquid Sodium/Molten Salt Systems–Step Change in the Receiver Heat Flux

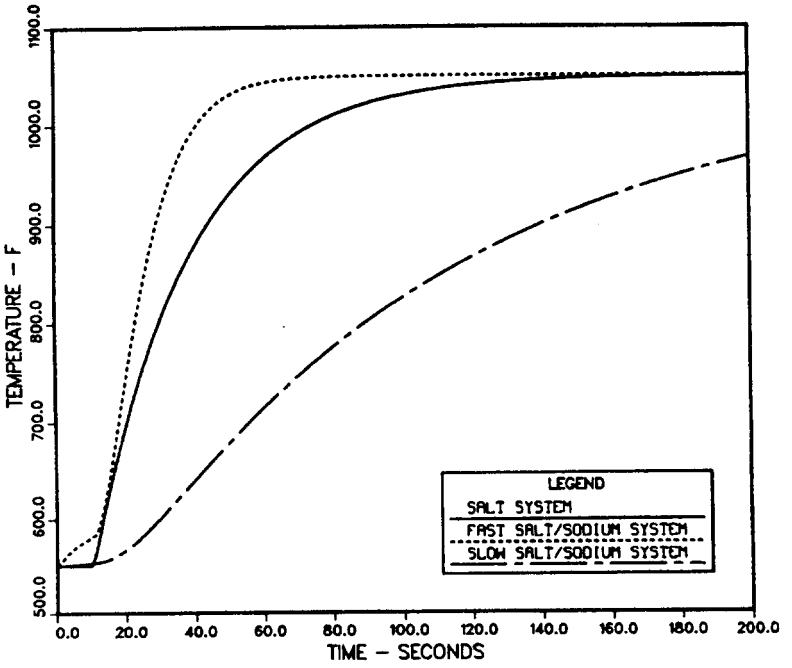

Figure 18. Comparison of the Delivered Molten Salt Temperatures for the Molten Salt and Liquid Sodium/Molten Salt Systems–Effect of Heat Exchanger Design Under a Step Flux Change

Salt temperature histories from the slow and fast sodium/salt systems are compared with the base case salt system. An examination of the time constants for the three curves indicates that the salt system is 3.9 times faster than the slow sodium/salt design but 1.6 times slower than the fast sodium/salt design. Hence it is difficult to draw general conclusions regarding the relative step flux startup times for the salt and sodium/salt systems without first specifying a sodium/salt heat exchanger design.

The comparison of Figure 18 is repeated in Figure 19 for the case when the flux is applied to the receivers over a 10 minute period rather than as a step. This is undoubtedly a more realistic startup condition for the two systems. The fast sodium/salt system responds more quickly than the salt system in the early time period. This is due primarily to the initial conditions selected for the heat exchanger and the inventory of 316 ° C sodium available for raising the salt temperature from 288 ° C to 316 ° C even before significant heat flux is applied. As time progresses, however, it becomes clear that the single most important parameter influencing the startup is the rate at which the heat flux is applied and not the thermal inertia inherent in the design. Even for the unrealistically bulky heat exchanger used in the simulation of the slow sodium/salt system the rate of salt temperature rise is nearly the same as the salt system or even the fast sodium/salt system. The major difference between the fast and slow sodium/salt system responses seems to occur as a result of the 28 ° C "head start" resulting from heat exchanger initial conditions.

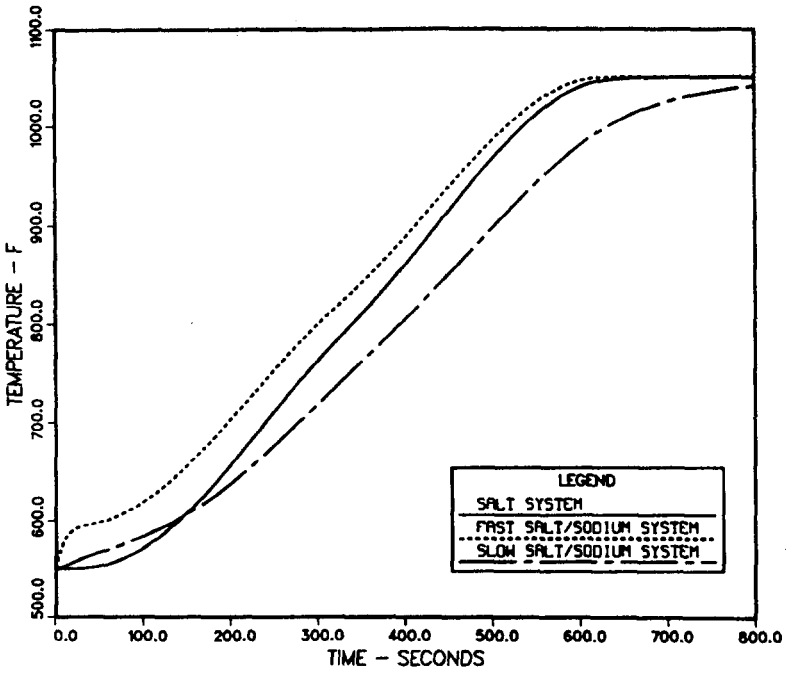

Figure 19. Comparison of Delivered Molten Salt Temperatures for the Molten Salt and Liquid Sodium/Molten Salt Systems–Effect of Heat Exchanger Design with a 10 Minute Flux Ramp

Summary

The numerical study presented in this chapter compares the relative startup times for the salt and sodium/salt systems. Only the effects of heat capacity were examined. Special delays in system startup due to operational constraints (e.g., salt or sodium safety issues, component automatic control, etc.) were not considered.

The key results from this chapter are:

1. For typical receiver designs, salt receivers are approximately 3.8 times slower in startup than sodium receivers when a step flux is applied. For more realistic (slower) applications of solar flux this difference in startup times becomes less.

2. It is virtually impossible to make sweeping conclusions regarding the relative step flux startup times for the complete salt and sodium/salt systems without first specifying a heat exchanger design.

3. Comparisons between the slow and fast sodium/salt system designs and the base salt system design indicate the importance of heat exchanger design in estimating relative startup times. For step flux startup, the salt system was found to be approximately 3.9 times faster than the slow sodium/salt design but 1.6 times slower than the fast salt/ system design.

4. For more realistic system startup involving slow application of the solar flux (i.e., over periods of time greater than 10 minutes), the startup times required for the salt and sodium systems are essentially the same regardless of design.

Economic Comparison

The system efficiency and system transient performance serve to establish the annual energy output of a particular system configuration. However, the value of a solar central receiver plant is determined by its levelized energy cost.

Annual Energy

The levelized energy cost, LEC, is calculated by the following equation:

$$LEC = \frac{(CC)(PCV)(FCR) + OM}{Annual\ Energy}$$

where,

LEC = levelized energy cost, \$/kWh
CC = plant capital cost, \$
PCV = factor to adjust capital cost reflecting expenditures over a three year construction period
FCR = fixed charge rate
OM = annual operations and maintenance charge, \$

The annual energy used in this report is calculated using the design point thermal power from the receiver less the thermal power equivalent of the electric power to run the major system pumps. Since tower heights differ between north and surround fields, the required pumping power to flow the molten salt heat transfer fluid through the receiver will vary. The sodium systems have a closed sodium heat transfer loop not connected to a large tank, which can be operated at the hydrostatic head. Therefore, the sodium receiver circulation pump has only to overcome the frictional pressure drop in the piping and receiver. However, sodium systems must include a molten salt circulation pump for cooling the sodium-to-salt heat exchanger. The annual energy is then:

Molten Salt:

$$AE = P_r - \frac{m_r(tht + 152)9.8}{(0.38)(0.8)(10^6)} H_y$$

Liquid Sodium:

$$AE = P_r - \frac{[(152m_r) + (64m_{hx})]9.8}{(0.38)(0.8)(10^6)} H_y$$

where,

AE = annual energy, MWh_t
P_r = receiver thermal power, MW_t

m_r = receiver fluid mass flow rate, kg/s
tht = receiver tower height, m
m_{hx} = heat exchanger salt mass flow rate, kg/s
H_y = number of operating hours per year

A constant head drop through the receiver of 152 meters is assumed for all receivers. The molten salt circulation pump for the sodium-to-salt heat exchanger is assumed to have a head of 64 meters. The pump efficiency is taken to be 0.8 and the thermal to electric conversion efficiency is taken to be 0.38.

It was thought that the parasitic pumping power requirements could be a deciding factor between system levelized energy costs. The greatest parasitic pumping power estimate is about 23 MW_t and the least about 10 MW_t. The parasitic pump power is a 2% effect, at best, on levelized energy cost. Therefore, the parasitic pumping power requirements are not a factor at the plant size considered in this report. Trace heating parasitics are not included since it was assumed there is no significant difference in the trace heating load required by each configuration.

Cost Estimates

The plant capital cost is calculated from cost models developed at SNLL based on Solar One data and cost estimates from reports[4,5,6]. Since many items do not vary in design from system to system, the majority of the capital cost is fixed. The fixed costs are:

Field Cost, FC: $\$204.6 \times 10^6$

Storage Cost, SC: $\$45.7 \times 10^6$

Electric Power Generation System Cost, EC: $\$15.0 \times 10^6$

Fixed Balance of Plant Cost, BC: $\$40.0 \times 10^6$

Receiver Tooling Cost, RTC: $\$0.435 \times 10^6$

Sodium Systems Only

Sodium Handling Cost, SHC: $\$0.466 \times 10^6$

Sodium Valve Cost, SVC: $\$0.2 \times 10^6$

Sodium Argon System Cost, SAC: $\$0.186 \times 10^6$

The rate at which indirect costs, IND, and engineering costs, ENG, were calculated are 0.2 and 0.05 respectively. The present capital value factor, PCV, and

the fixed charge rate, FCR, are 1.0318 and 0.0615 respectively. The costs that vary from design to design are:

Absorber Panel Cost, RPC

Receiver Insulation Cost, RIC

Receiver Shipping Cost, RSC

Receiver Surge Tank Cost, RSTC

Receiver Erection Cost, REC

Tower Cost, TC

Cavity Receivers Only

Cavity Structure Cost, RCC

Sodium Systems Only

Sodium-to-Salt Heat Exchanger Cost, HXC

Sodium Circulation Pump Cost, SPC

Molten Salt Circulation Pump Cost, CPC

Molten Salt Systems Only

Molten Salt Receiver Pump Cost, RPC

It was decided to estimate the cost the external and cavity receiver designs each with molten salt and liquid sodium as the receiver coolant. The unit absorber cost for sodium receivers is less by a factor of 0.55 than the unit absorber cost for molten salt receivers because of the material cost difference between 316 stainless steel and Incoloy 800. The capital cost, CC, is calculated as follows:

$$CC = ST + (ST \times IND) + (ST \times ENG)$$

where the subtotal cost, ST, is calculated for the various system designs as follows:

Molten Salt External Receiver

$$ST = FXC + VC + RPC$$

Liquid Sodium External Receiver

$$ST = FXC + FSC + VC + VSC$$

Molten Salt Cavity Receiver

$$ST = FXC + RCC + VC + RPC$$

Liquid Sodium Cavity Receiver

$$ST = FXC + FSC + RCC + VC + VSC$$

where,

$$FXC = FC + SC + EC + BC + RTC$$

$$FSC = SHC + SVC + SAC$$

$$VC = RPC + RSC + RSTC + REC + TC + RIC$$

$$VSC = HXC + SPC + CPC$$

And finally, the operations and maintenance cost, OM, is fixed for all systems at $\$8.0 \times 10^6$ per year.

Results

The levelized energy costs (LEC) for twelve system design cases were generated. The objective in this cost exercise was to calculate numbers that reflected the relative costs of the various system components so that comparisons may be made. Since the absolute value of the levelized energy cost can be misleading, only the levelized energy costs normalized to the greatest levelized energy cost are reported. The key system design characteristics and normalized LEC for each case are presented in Table VIII. The normalized LEC as a function of peak flux is plotted in Figure 20.

In Table VIII, external receivers are always matched to surround fields and cavity receivers are always matched to north fields. The receiver power is the power at the base of the receiver and varies from design to design because of varying receiver and field efficiencies. The tower height is the height of the tower from the ground to the base of the receiver. The system efficiencies for cavity receivers presented in the System Efficiency chapter are all for a receiver optical

Table VIII. System Levelized Energy Cost

Case No.	Receiver Configuration	Peak Flux MW_t/m^2	Receiver Power MW_t	Receiver Area m^2	Tower Height m	Normalized LEC
1	external molten salt	0.24	480	3563	157	0.890
2	external molten salt	0.70	520	1539	179	0.767
3	external molten salt	1.78	522	679	183	0.739
4	external liquid sodium	0.24	480	3563	157	0.874
5	external liquid sodium	0.70	520	1539	179	0.767
6	external liquid sodium	1.78	522	679	183	0.745
7	cavity molten salt	0.24	548	7477	346	1.000
8	cavity molten salt	0.62	593	2406	352	0.774
9	cavity molten salt	1.82	565	681	353	0.755
10	cavity liquid sodium	0.24	550	7477	351	0.937
11	cavity liquid sodium	0.62	593	2406	352	0.755
12	cavity liquid sodium	1.82	565	681	353	0.752

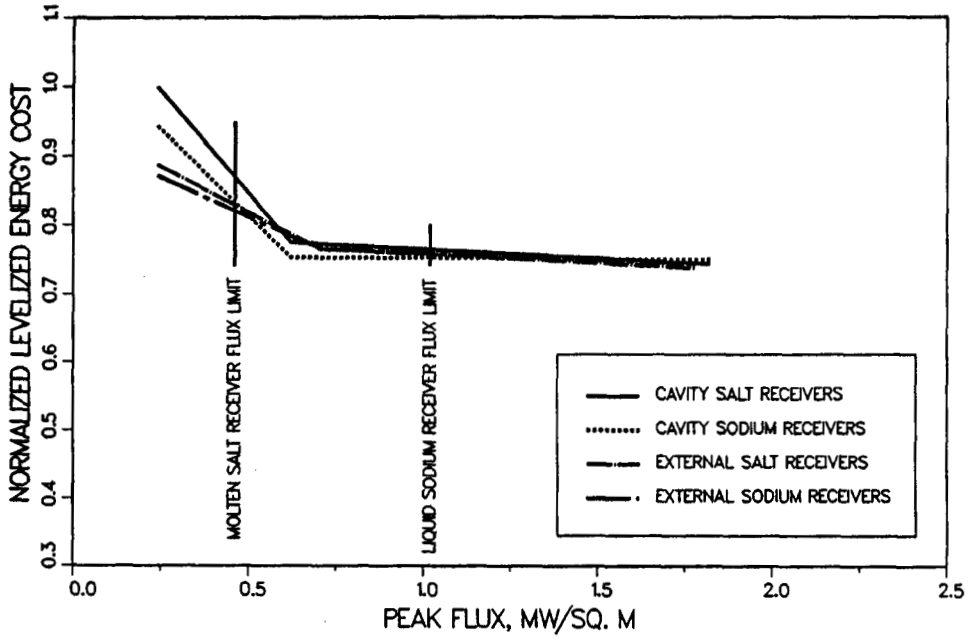

Figure 20. Economic Comparison of Heliostat Field Receiver Configurations

height of 450 meters; the receiver optical height is the distance from the center of the receiver to the heliostat pivot point. This tall tower is extremely expensive; around \$120 x 10^6. Therefore, the cavity receiver tower heights were optimized to determine the minimum levelized energy cost as described in Appendix B.

Figure 20 shows that the levelized energy costs for all system configurations become essentially the same at peak flux levels above 0.7 MW_t/m^2. However, below 0.7 MW_t/m^2 the systems separate in levelized energy cost. The peak flux limits as determined in the System Efficiency chapter are marked on Figure 20. The corresponding normalized LEC's for a molten salt cavity receiver and external liquid sodium receiver are 0.88 and 0.75 respectively. This means that the

surround field/liquid sodium receiver configuration delivers energy that is 14% less expensive than the north field/molten salt cavity receiver configuration.

Due to the short period of time (2 months) available for preparing this report to meet internal deadlines, and the fact that information arrived from many sources at different times, it was not possible to obtain cost estimates for the systems at the nominal molten salt and liquid sodium peak flux levels of 0.46 and 1.02 MW_t/m^2 as determined in the System Efficiency chapter. However, this does not prevent comparisons illustrating the factors affecting system levelized energy cost. Table IX presents a breakdown of the variable costs for Cases 2, 6, 8 and 12 (Table VIII) which are used to represent systems at molten salt peak flux levels and liquid sodium peak flux levels.

Table IX. Variable Cost Breakdown
(all costs are in millions of dollars)

Receiver Configuration	External		Cavity	
Receiver Fluid	Salt	Sodium	Salt	Sodium
Peak Flux	0.62	1.78	0.62	1.78
	Case 2	Case 6	Case 8	Case 12
Receiver				
Absorber	14.3	3.4	22.3	3.5
Insulation	0.8	0.5	1.0	0.5
Shipping	0.3	0.1	0.4	0.1
Surge Tanks	3.0	3.4	3.3	3.6
Erection	11.2	5.0	17.5	5.0
Cavity Structure	0.0	0.0	7.6	2.2
Tower	6.0	5.9	42.2	42.7
Heat Transport				
Sodium-to-Salt HX	0.0	7.0	0.0	7.2
Sodium Handling Equipment	0.0	0.5	0.0	0.5
Sodium Argon Gas System	0.0	0.2	0.0	0.2
Sodium Valves	0.0	0.2	0.0	0.2
Molten Salt Receiver Pump	1.0	0.0	1.4	0.0
Molten Salt HX Circ. Pump	0.0	0.9	0.0	1.0
Capital Cost*	427.8	417.7	502.1	467.2

*not a sum of the above numbers

According to Table IX, the major cost differences between a surround field/external liquid sodium receiver system and a north field/molten salt cavity receiver system are the absorber panel cost and the tower cost. The molten salt cavity receiver absorber cost is high because considerably more absorber area

is required due to the reduced flux level, and because a more expensive tube material, Incoloy 800, is used. The tower cost is higher for a north field configuration than a surround field because a higher tower is required in order to achieve a reasonable system efficiency. The cost of the cavity structure and sodium-to-salt heat exchanger seem to be of secondary concern. The remaining items have a negligible effect.

Sodium-to-Salt Heat Exchanger

The cost of the sodium-to-salt heat exchanger is particularly uncertain since it is unknown how one would be constructed. The primary cause of this uncertainty is that the reaction between sodium and molten nitrate salts at high temperature has not been studied experimentally. However, thermochemical calculations show that molten nitrate salts should react exothermically with liquid sodium.[7] Therefore, it then seems appropriate to conduct a sensitivity study to see how the cost of the sodium-to-salt heat exchanger cost affects the levelized energy cost. Table X shows how the normalized LEC for a surround field/external liquid sodium receiver for a peak flux of 1.02 MW_t/m^2 varies with an increasing sodium-to-salt heat exchanger cost.

Table X. The Effect of the Sodium-to-Salt Heat Exchanger Cost on the Levelized Energy Cost

Heat Exchanger Cost $ x 10^{-6}	Normalized LEC
7.0	0.759
50.0	0.831
60.0	0.850
70.0	0.865
80.0	0.881

The normalized LEC for comparative north field/molten salt cavity receiver at 0.46 MW_t/m^2 is 0.865

Table X shows that if the cost of the sodium-to-salt heat exchanger increases by a factor of 10 or \$70 x 10^6, the levelized energy cost for the surround field/external liquid sodium receiver is essentially equivalent to the levelized energy cost for the north field/molten salt cavity receiver. However, the capital cost difference required for equivalence is not greater than the probable level of relative uncertainty in the cost estimates which is +/- 25% or more. Therefore, it is entirely possible that the cost uncertainties associated with the sodium-to-salt heat exchanger combined with other cost uncertainties could eliminate the cost advantage of the surround field/liquid sodium receiver configuration.

Summary

Cost estimates are fertile ground for controversy, but a necessary factor in any evaluation of solar thermal central receivers. The cost estimates presented in

this chapter are intended to show relative cost differences and not absolute cost differences. With this in mind, the following conclusions are made:

1. The surround field/liquid sodium external receiver configuration delivers energy at a levelized energy cost approximately 14% below that of the north field/molten salt cavity receiver configuration.
2. The majority of this cost difference can be attributed to the more expensive absorber and tower cost of the molten salt receiver. The absorber cost is higher because of the lower average flux at which a molten salt receiver must be operated and the more expensive material selected for absorber fabrication. The tower cost is greater because a higher tower is required to achieve the cost optimal system efficiency.
3. Uncertainties in some system component costs, particularly the sodium-to-salt heat exchanger, may eliminate the cost differential between the two system configurations.
4. Differences in parasitic pumping power requirements between the two system configurations are not significant.

Suggestions for Extension of Study

The preceeding three chapters have covered many aspects of solar thermal central receiver evaluation. This chapter will briefly discuss some issues that were not examined in this report.

Receiver Design and Performance

Absorber Area–The receiver designs presented in this report were generated by the computer program DELSOL2. As noted in the chapter on System Efficiencies, DELSOL2 tends to design cavity receivers with greater absorber surface area than external receivers for the same peak flux service. The greater the cavity absorber area, the greater the total internal area of the cavity. Since the convective losses of the cavity receivers are calculated based on the entire internal area of the cavity, this cavity receiver design method seems to penalize cavity receivers relative to external receivers. An investigation into cavity receiver design practices should illuminate those factors which contribute to excessive cavity receiver absorber area.

Receiver Absorber Tube Length–The length of receiver absorber tubes is not an issue in this report. However for the actual fabrication of a receiver, the absorber tubes are probably limited to a maximum of 24 to 30 meters (80 to 100 feet) due to manufacturing and shipping limitations. Table XI lists the receiver heights for the six different receivers compared in this report. The receiver height is equivalent to the active tube length since the tubes are oriented vertically. The tube stated length maximum suggests most of the receivers considered in this report cannot be constructed. However, since it is absorber area and not height that is most important, there is no reason why a receiver for a particular peak flux cannot be built wider to accomodate a height limitation. The effects ought to be minimal for external receivers since the field and receiver efficiencies are not strongly dependent on absorber height.

Table XI. Receiver Heights

Receiver	Height, meters
External, 0.24 MW_t/m^2 peak flux	63.0
External, 0.70 MW_t/m^2 peak flux	35.0
External, 1.78 MW_t/m^2 peak flux	12.0
Cavity, 0.24 MW_t/m^2 peak flux	59.5
Cavity, 0.62 MW_t/m^2 peak flux	38.3
Cavity, 1.82 MW_t/m^2 peak flux	26.0

Cavity receivers ought to be affected more strongly, since decreasing the absorber height will increase the aperture size and/or increase the minimum heliostat field radius. Each effect will act to reduce the system efficiency. Therefore, it is expected that cavity receivers will fare worse in the event of an absorber tube length limit.

Receiver Part-Load Performance–It was assumed when calculating the system efficiencies that design point receiver performance can be used rather than annual receiver performance and still result in a meaningful comparison of system efficiencies. The design point receiver performance is used because De Laquil and Anderson provided only design point receiver performance in their report. Since receivers seldom operate near their design point, the annual receiver performance is dependent on the receiver part-load performance characteristics. It is entirely possible that cavity and external receivers have different part-load performances, which when integrated over the year, could change the relative system efficiencies presented in Figure 7.

System Issues

Plant Size and Modularity–This report examined systems having thermal output powers between 500 and 600 MW_t and utilizing a single field/receiver combination for a single thermal storage and electric generation system. Other power levels and the advantages, if any, of modularity were not examined here.

Control Strategy–The transient performance analysis of the north field/molten salt cavity receiver and surround field/liquid sodium external receiver was conducted assuming a very simple temperature control strategy. It was not possible, given the level of detail and time available, to assess transient performance of these two systems under realistic startup and operating conditions.

Other System Configurations–Figure 20 and Table VIII contain two heliostat field/receiver configurations in addition to the two configurations of primary interest in this report. These two additional configurations are the surround field/external molten salt receiver and the north field/liquid sodium cavity receiver configurations. It is typically assumed that a molten salt receiver must be a cavity receiver because it allows the large absorber to be kept warm overnight for faster morning startup. The sodium receiver is typically assumed to be an external receiver since its small size and light weight allow it to be drained of sodium at night and left to cool to ambient with no penalty in morning startup time.

If the molten salt receiver could be operated as an external receiver, it appears this configuration would be cost competitive with any sodium based design. If it were decided that a cavity structure on a sodium receiver was necessary for thermal protection, it appears there is little or no cost penalty for this addition. Though this report has concentrated on the other two configurations, the reader

should be well aware that other options exist within the range of normalized levelized energy costs reported herein.

Summary

The key results of this chapter are:

1. Receiver design methods require review and improvement. Cavity receiver design in particular appears to be less well understood and more complicated than external receiver design.

2. Configuration options other than the surround field/liquid sodium external receiver and the north field/molten salt cavity receiver may provide better economics or operating flexibility.

Conclusion

In the preceeding report, each chapter contains a set of conclusions pertaining only to that chapter. The major conclusions of this report are presented here as follows:

1. Generic north heliostat field/cavity receiver configurations are 6 to 10 percent more efficient than a generic surround field/external receiver configuration. This is due mostly to the better cosine efficiency of a north field.

2. There is little difference in the transient performance of a molten salt receiver compared to a sodium receiver connected to a sodium-to-salt heat exchanger. This is largely because the system time constants are controlled by the heat transfer capability and thermal inertia of the molten salt.

3. The surround field/liquid sodium external receiver configuration may provide energy at a 14 percent lower levelized energy cost than a north field/molten salt cavity receiver configuration. In spite of the efficiency advantage inherent in the north field/cavity receiver configuration, the higher capital cost of absorber and tower act to increase its levelized energy cost to above that of a surround field/external receiver configuration. However, the cost advantage of the surround field/liquid sodium external receiver is not conclusive because of uncertainties in system components, notably the sodium-to-salt heat exchanger.

Recommendations

Based on the results of this study,

1. It is recommended that the surround field/liquid sodium external receiver configuration be considered as the reference configuration which will serve as a basis of comparison in future, more detailed studies.

2. It is recommended that more effort be placed on the improvement of cavity receiver design and performance estimates than on external receiver design and performance.

3. It is recommended that investigations into the design, construction and operation of a sodium-to-salt heat exchanger continue.

APPENDICES

APPENDIX A–LUMPED PARAMETER MODEL FORMULATION

Lumped parameter model schematics for the receiver and counterflow HX are shown in Figures A-1 and A-2 respectively.

The assumptions used in formulating the two lumped parameter models are summarized as follows:

1. The average temperatures for the receiver front half tube (F), the receiver back half tube (B), the receiver fluid (R), the heat exchanger flowing sodium (N), the heat exchanger sodium/salt tube wall (W), the heat exchanger flowing salt (S), and the heat exchanger outside shell (O) are characterized by the single lumped temperatures $\overline{T}_F, \overline{T}_B, \overline{T}_R, \overline{T}_N, \overline{T}_W, \overline{T}_S$, and $\overline{T}_O$ respectively. These lumped temperatures vary with time but not axial distance.

2. All fluid properties and heat transfer coefficients are constant and are evaluated at the mean steady state operating temperature which is 800 ° F for both the salt and the sodium.

3. Receiver losses are not included in the study.

4. The back side of the receiver tube is perfectly insulated.

5. The heat exchanger is perfectly insulated.

6. A uniform flux is applied to the receiver (.3 MW_t/m^2 for the salt receiver and .6 MW_t/m^2 for the sodium receiver).

7. For the purpose of computing shell and tube heat transfer conductances, the counterflow heat exchanger is configured as an annulus with sodium flowing in the tube and salt flowing in the annular or shell side.

8. Heat transfer coefficients for the salt are determined from the Dittus Boelter heat transfer correlation[16] based on the hydraulic diameter of the flow path cross-section.

9. Heat transfer coefficients for the sodium are determined from the liquid metal heat transfer correlation for interior tube flow by Lyon[17] and Dwyer[18].

Assumptions 2 through 9 are expected to be relatively insignificant compared to assumption 1. The importance of assumptions 2 through 9 were evaluated parametrically in order to determine if they biased one system over another. No strong biases were evident. The major assumption, the notion that long components and flow streams can be "lumped" will be evaluated in the next section.

The lumped parameter models for the seven major heat capacities in the receiver and heat exchanger may be written directly from a simple conservation of energy principle.

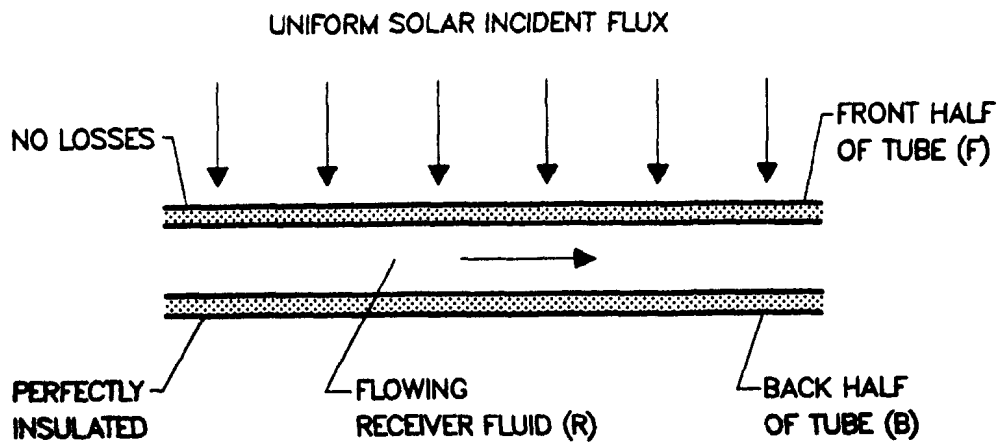

Figure A-1. Lumped Receiver Model

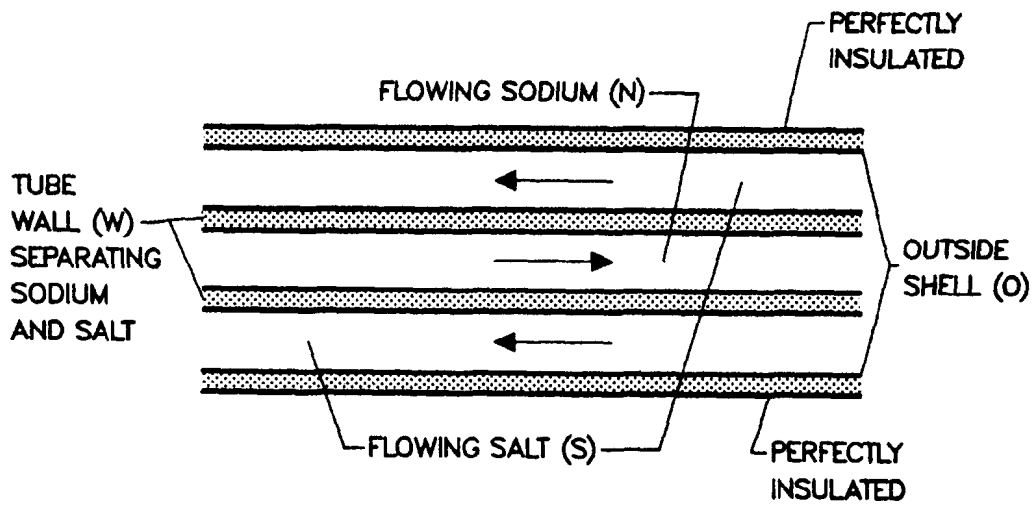

Figure A-2. Lumped Counterflow Heat Exchanger Model

Receiver front wall:

$$(mc)_F \frac{d\overline{T}_F}{dt} = q'' A_{FA} - (hA)_{FR}(\overline{T}_F - \overline{T}_R) \quad (1)$$

Receiver back wall:

$$(mc)_B \frac{d\overline{T}_B}{dt} = (hA)_{BR}(\overline{T}_R - \overline{T}_B) \quad (2)$$

Receiver fluid:

$$(mc)_R \frac{d\overline{T}_R}{dt} = (hA)_{FR}(\overline{T}_F - \overline{T}_R) + (hA)_{BR}(\overline{T}_B - \overline{T}_R) - (\dot{m}c)_R(T_{RI} - T_R) \quad (3)$$

Sodium in HX:

$$(mc)_N \frac{d\overline{T}_N}{dt} = (hA)_{WN}(\overline{T}_W - \overline{T}_N) + (\dot{m}c)(T_{NI} - T_N) \quad (4)$$

HX tube wall:

$$(mc)_W \frac{d\overline{T}_W}{dt} = (hA)_{WN}(\overline{T}_N - \overline{T}_W) + (hA)_{WS}(\overline{T}_S - \overline{T}_W) \quad (5)$$

Salt in HX:

$$(mc)_S \frac{d\overline{T}_S}{dt} = (hA)_{OS}(\overline{T}_O - \overline{T}_S) + (hA)_{WS}(\overline{T}_W - \overline{T}_S) + (\dot{m}c)_S(T_{SI} - T_S) \quad (6)$$

HX outer shell:

$$(mc)_o \frac{dT_O}{dt} = (hA)_{OS}(\overline{T}_S - \overline{T}_O) \quad (7)$$

In equations (1) through (7) the notation $(mc)_i$ refers to the heat capacity (product of mass and specific heat) for component i, i=F, B, R, N, W, S, and O. Constants $(hA)_{ij}$ are the heat transfer conductances (product of heat transfer coefficient and surface area) between components i and j. The constants $(mc)_i$ are the product of mass flow rate and heat capacity for fluid i, i = R, N, S. The remaining constants in the equations are defined as follows:

q'' = uniform heat flux per unit area

A_{FA} = projected absorbing surface for q''

T_{RI} = constant receiver inlet temperature which is 288 ° C (550 ° F) for the salt receiver, 316 ° C (600 ° F) for the sodium receiver

T_{SI} = constant salt heat exchanger inlet temperature (288 ° C)

The outlet receiver temperature, T_R for the sodium/salt system is identical to the inlet sodium heat exchanger temperature since the receiver and heat exchanger are configured in a series arrangement. T_R is estimated using a first order approximation which assumes a linear temperature variation for the receiver fluid along the length of the tube. Hence T_R is given by:

$$T_R = 2\overline{T}_R - T_{RI} \tag{8}$$

The outlet temperature of the salt from the heat exchanger is estimate using a similar first order approximation:

$$T_S = 2\overline{T}_S - T_{SI} \tag{9}$$

Differential and algebraic equations (1) through (9) completely describe the lumped parameter model for the sodium/salt system in terms of the eight unknowns $\overline{T}_F, \overline{T}_B, \overline{T}_R, \overline{T}_N, \overline{T}_W, \overline{T}_S, \overline{T}_O, T_R$, and T_S. Fluid properties for R subscripted quantities are those of sodium. The initial conditions for the model are designed to simulate a prestart of condition in which the receiver is at a uniform temperature of 316 ° C and the heat exchanger (including sodium) is at a uniform temperature of 288 ° C, hence:

$$\overline{T}_F(0) = \overline{T}_B(0) = \overline{T}_R(0) = T_R(0) = 316°C$$

and

$$\overline{T}_N(0) = \overline{T}_W(0) = \overline{T}_S(0) = \overline{T}_O(0) = T_S(0) = 288°C$$

The model attempts to predict the time required to achieve steady state 566 ° C (1050 ° F) salt delivery once a heat flux, q'', is applied to the receiver.

Differential and algebraic equations (1), (2), (3) and (8) completely describe the lumped parameter model for the salt system in terms of four unknowns $\overline{T}_F, \overline{T}_B. \overline{T}_R$, and T_R. In this case the R subscripted quantities are those of molten salt and the initial conditions correspond to a prestart condition in which the receiver is at a uniform temperature of 288 ° C, i.e., $\overline{T}_F(0) = \overline{T}_B(0) = \overline{T}_R(0) = T_R(0) = 288°C$. Here again, the model attempts to predict the time required to achieve steady state 566 ° C salt delivery once a heat flux, q'', is applied to the receiver.

The differential equations which comprise the lumped receiver and heat exchanger models were programmed for solution using Fortran coding and the explicit ordinary differential equation solver ODE[19].

Assessment of the Lumped Parameter Assumption

If the purpose of the study were to accurately describe the thermal history of fluid flow and fluid containment as a function of space and time, clearly the lumped model described in the previous section would be inadequate. The objective here, however, is to develop a model which exhibits the same startup time constant as the real system. The ability of the lumped parameter models to predict correct startup time constants can only be evaluated through a comparison with actual experimental data, or with more sophisticated models.

The accuracies of the lumped parameter models for the salt and sodium receivers were tested against the more accurate code DRAC (Dynamic Receiver Analysis Code). DRAC is a user-friendly interface for the more general code TOPAZ (Transient One-Dimensional Pipe Flow Analyzer). DRAC and TOPAZ are documented in references 20 and 21 respectively.

The DRAC/TOPAZ computer code models all the pertinent one-dimensional-transient fluid flow and two-dimensional-transient heat conduction physics associated with a single receiver tube irradiated by a time-dependent solar flux. The code conserves continuity, momentum, and energy for the flowing fluid (e.g., sodium or molten salt) and computes local quasi-steady forced convection heat transfer coefficients and friction factors as a function of the local temperature dependent fluid properties.

A "base case" receiver tube design was proposed for both a typical salt receiver and a typical sodium receiver. Parameters (e.g., flow rate, heat flux, tube inside diameter and outside diameter, etc.) for the two base cases were derived from actual system designs and tested hardware configurations. The parameters are discussed in greater detail in the Transient Performance chapter.

Figure A-3 compares the lumped model and DRAC/TOPAZ predicted receiver outlet temperature responses for the salt base case. In each model it is assumed that salt flows at the steady state design flow rate throughout the transient. The salt inlet temperature (and hence initial tube wall temperatures) is 288 ° C. At t=10 seconds the front half of the receiver tube is hit with a step change in uniform receiver flux from .0 to .3 MW_t/m^2.

Figure A-4 displays the identical comparison for the sodium receiver. In this case the flux level is .6 MW_t/m^2 and the receiver inlet temperature is 316 ° C.

The lumped models for the sodium and salt receivers failed to predict the precise steady state outlet temperatures due to the fact that constant fluid properties (ρ and c) were used in the calculations rather than accounting for the actual fluid property dependence. As expected the lumped model does not predict the precise receiver temperature history for the two receivers. However, the response time constants for the two models and the two receivers appear to be relatively consistent. Here we define the time constants for the step change in receiver flux

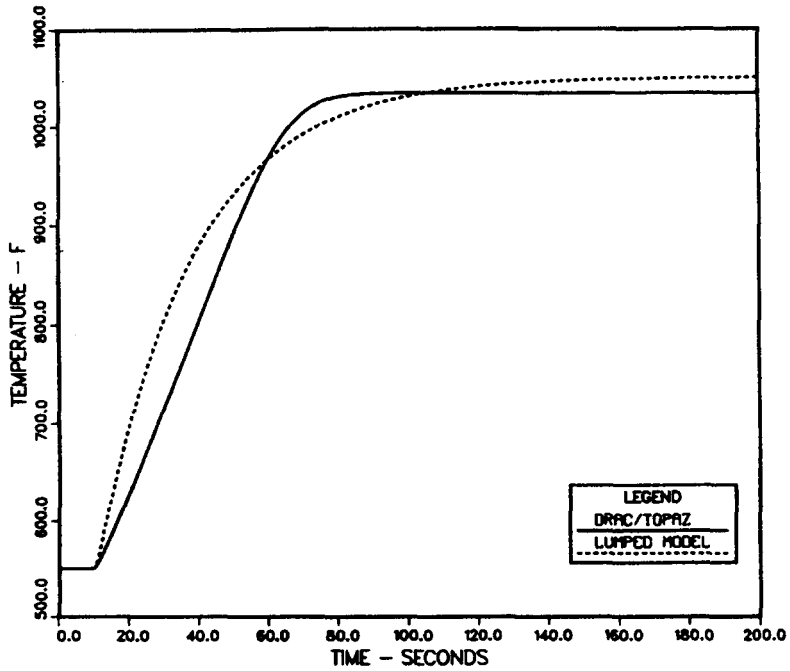

Figure A-3. Comparison of Molten Salt Receiver Outlet Temperature Transients from Lumped and Distributed Models–Base Case

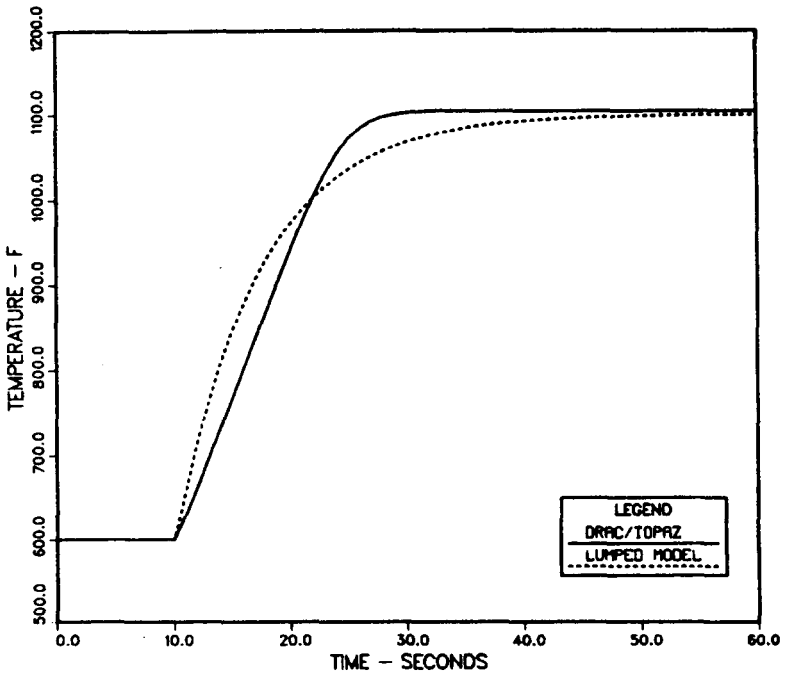

Figure A-4. Comparison of Liquid Sodium Receiver Outlet Temperature Transients from Lumped and Distributed Models–Base Case

as the time required for the receiver outlet temperature to cover 63.2% of the entire temperature excursion.

Table A-I summarizes the time constant comparisons for the two models and for the salt and sodium base case receivers. The time constant errors induced by using the lumped model are on the order of 22% for both the salt and sodium receivers. Hence while the lumped model is a crude one, its use does not appear to bias errors in favor of the salt or sodium system. The lumped model approach would not be recommended for predicting precise system response in individual salt and sodium systems but for the purpose of comparing the salt system response relative to the sodium/salt system response these simplified models would appear to have value. Consistent and obvious differences between startup times for the two systems of interest should be replicated by the lumped parameter models.

Table A-I. Time Constant Comparison for the Base Case Salt and Sodium Receivers

	Lumped Model	DRAC Model	Percent Deviation
Molten Salt Receiver	28.2 sec	36.0 sec	-21.7%
Liquid Sodium Receiver	7.4 sec	9.6 sec	-22.9%

Table A-I indicates that both the lumped and DRAC/TOPAZ models predict the base case salt receiver response to be 3.8 times slower than the sodium receiver response. This, of course, is due to the increased length of the salt receiver tubing which is required to absorb the lower level solar flux. It should be pointed out, however, that in actual practice, a receiver would never be started up with a step change in flux from zero to the design point. Damage to the receiver would most certainly take place in such a situation. In practice the receiver flux would be increased much more slowly. If the same scenario for applying flux to the salt and sodium receivers is used, one would expect the startup time differences to decrease in situations where the flux is applied slowly. In the limit where the flux is increased to the design point over several hours, one would expect no startup time differences for the two receivers. If the step increase in flux were used, the maximum difference in startup times would result. Similar arguments apply for the comparison between the salt system and the salt/sodium system (i.e., the addition of the heat exchanger). The effect of startup flux rate and other heat exchanger parameters are discussed in the main body of the text.

The lumped parameter models for the receiver and heat exchanger appear to have considerable value when assessing the relative startup of the salt and sodium/salt systems and components. This was demonstrated in the case of salt and sodium receivers by comparing the lumped parameter step flux startup responses to those of the more precise DRAC/TOPAZ receiver model. While the precise outlet receiver temperature history varied, the lumped parameter model

consistently produced first order time constant responses which were within 22% of the actual responses. Furthermore, the lumped analysis did not bias salt components over sodium components or vise versa.

APPENDIX B–OPTIMIZATION OF THE NORTH FIELD TOWER HEIGHTS

The high cost of receiver towers may lead to a reduction in tower height below that where the system performance is a maximum if such a move results in a lower delivered levelized energy cost. This condition exists in this study.

The system efficiencies were determined without regard to cost. The result for north field/cavity receiver configurations requires 450 meter tower costing around \$120 x 10^6. Since the total system cost for a north field/cavity receiver configuration is around \$500 x 10^6, reductions in the tower cost can have a noticeable impact on the levelized energy cost.

The approach taken here to determine the optimal tower height for the north field/cavity receiver configurations was to determine the levelized energy cost associated with reducing the tower height. This was done by rewriting the equation for the levelized energy cost in terms of the tower height as follows:

$$LEC = \frac{(CC_o + C_{tow})(PCV)(FCR) + OM}{P_r(PRF) - PAR}$$

where

CC_o = plant capital cost excluding the tower capital cost
C_{tow} = tower capital cost
PCV = factor to adjust capital cost which reflects construction expenditures over a three year period
FCR = fixed charge rate
OM = annual operations and maintenance charge
P_r = receiver power at a tower height of 450 meters
PRF = power reduction factor for calculating the receiver power at tower heights below 450 meters
PAR = parasitic power of the pumps which are a function of tower height only for the salt receivers.

The power reduction factor, PRF, is a function of tower height and is derived from data presented by De Laquil and Anderson[1]. De Laquil and Anderson presented the heliostat field efficiency as a function of tower height as shown in Figure B-1. The heavy solid curve was hand-fitted to the data. Points on this curve were read and normalized by the annual field efficiency at a tower height of 450 meters producing what is called the power reduction factor. This normalized data was used to develop a second order polynomial equation approximating the data. The power reduction factor as a function of tower height is then:

$$PRF = a_2 THT^2 + a_1 THT + a_0$$

where

THT = tower height as determined by DELSOL2
a_2 = -8.2489 x 10^{-6}
a_1 = 0.006777
a_0 = -0.3856

The LEC was calculated at 5 meter intervals from 200 meters to 450 meters for all the cavity receiver configurations. The tower height and reduced power level from the receiver (P_r x PRF) at the minimum LEC was used as input to the cost algorithms presented in the Economic Comparisons chapter to generate a more accurate LEC.

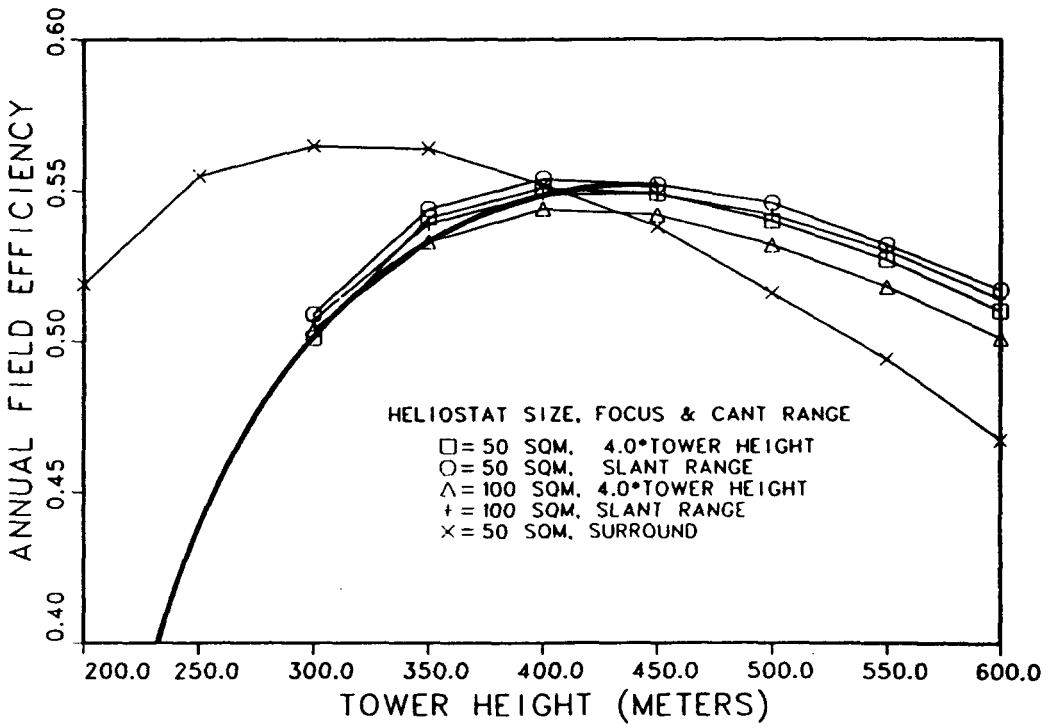

Figure B-1. Reduction in Field Performance as a Function of Tower Height

REFERENCES

1. P. De Laquil III and J. V. Anderson, "The Performance of High- Temperature Central Receiver Systems," SAND84-8233, Sandia National Laboratories, Livermore, CA, July 1984.

2. T. A. Dellin, M. J. Fish, and C. L. Yang,"A User's Guide for DELSOL2: A Computer Code for Calculating the Optical Performance and Optimal System Design for Solar Thermal Central Receiver Plants," SAND81-8237, Sandia National Laboratories, Livermore, CA, August 1981.

3. "Conceptual Design of Advanced Central Receiver Power System," DOE/ET/20314-1/2, Martin Marietta Corporation, Denver, CO, September 1979.

4. "Preliminary Design of Solar Central Receiver for a Site- Specific Repowering Application (Saguaro Power Plant)," DE-FCO3-82SFA11675, Arizona Public Service Co., September 1983.

5. "The Carrisa Plains Solar Central Receiver Project," ESG-84-14, Arco Solar Industries, Bechtel, PG&E, and Rockwell International, 1984.

6. H. F. Norris, "DELSOL2 Cost Default Recommendations and Cost Algorithm Modification," internal SNLL memo to P. K. Falcone dated February 20, 1985.

7. R. W. Bradshaw, "Reactions Between Liquid Sodium and Nitrate Salt," internal SNLL memo to J. J. Bartel dated January 30, 1985.

8. K. W. Battleson et al. "1980 Solar Central Receiver Technology Evaluation," SAND80-8235, Sandia National Laboratories, Livermore, CA, October 1980.

9. "Conceptual Design of Advanced Central Receiver Power Systems Sodium-Cooled Receiver Concept," SAN-1483-1/2, Rockwell International, Energy Systems Group, Canoga Park, CA, March 1979.

10. G. Carli, "Phase 1–Final Report, Molten Salt Solar Receiver Subsystem Research Experiment," SAND82-8180, Foster-Wheeler Development Corporation, Livingston, NJ, November 1982.

11. "Molten Salt Receiver Subsystem Research Experiment, Final Report Phase I," SAND82-8178, Babcock and Wilcox, Barberton, OH, November 1982.

12. M. Abrams, "RADSOLVER–A Computer program for Calculating Spectrally-Dependent Radiative Heat Transfer in Solar Cavity Receivers," SAND81-8248, Sandia National Laboratories, Livermore, CA, September 1981.

13. A. F. Emery, "Instruction Manual for the Program SHAPEFACTOR," SAND80-8027, Sandia National Laboratories, Livermore, CA, October 1980.

14. D. L. Siebers and J. S. Kraabel, "Estimating Convective Energy Losses from Solar Central Receivers," SAND84-8717, Sandia National Laboratories, Livermore, CA, April 1984.

15. B. L. Kistler, "Allowable Peak Flux Limits on Receiver Tubes Based on Fatigue Considerations," internal SNLL memo to S. E. Faas dated March 6, 1985.

16. F. W. Dittus and L.M.K. Boelter, University of California (Berkeley) Pub. Eng., Vol 2, p. 443, 1930.

17. R. N. Lyon, Liquid Metals Handbook, 3rd ed., Washington, D.C. Atomic Energy Commission and Department of the Navy, 1952.

18. O. E. Dwyer, "Liquid-Metal Heat Transfer", Chapt. 5, Sodium and NaK Supplement to the Liquid Metals Handbook, 1970 ed., Washington, D.C., Atomic Energy Commission.

19. L. F. Shampine and M. K. Gordon, "Subroutine ODE," SAND76-8209, Edited by T. H. Jefferson, Sandia National Laboratories, Livermore, CA, October 1977.

20. W. S. Winters, "DRAC-A User Friendly Computer Code for Modeling Transient Thermalhydraulic Phenomena in Solar Receiver Tubing," SAND82-8744, Sandia National Laboratories, Livermore, CA, January 1983.

21. W. S. Winters, "TOPAZ-A Computer Code for Modeling Heat Transfer and Fluid Flow in Arbitrary Networks of Pipes, Flow Branches, and Vessels," SAND83-8253, Sandia National Laboratories, Livermore, CA, January 1984.

February 11, 1986
UNLIMITED RELEASE
INITIAL DISTRIBUTION

U.S. Department of Energy (6)
Forrestal Building, Room 5H021
Code CE-314
1000 Independence Avenue, S.W.
Washington, D.C. 20585
Attn: H. Coleman
S. Gronich
B. Kessler
F. Morse
M. Scheve
R. Shivers

U.S. Department of Energy
Forrestal Building, Room 5H095
Code CE-33
1000 Independence Avenue, S.W.
Washington, D.C. 20585
Attn: C. Carwile

U. S. Department of Energy (2)
P.O. Box 5400
Albuquerque, NM 87115
Attn: D. Graves
J. Weisiger

U.S. Department of Energy (2)
1333 Broadway
Oakland, CA 94612
Attn: R. Hughey
M. Lopez

University of California
Environmental Science and Engineering
Los Angeles, CA 90024
Attn: R. G. Lindberg

University of Houston
Solar Energy Laboratory
4800 Calhoun
Houston, TX 77704
Attn: A. F. Hildebrandt

AMFAC
P.O. Box 3230
Honolulu, HI 96801
Attn: G. E. St. John

ARCO Solar
Route 1
P. O. Box 292
Fellows, CA 93224
Attn: M. Curley

ARCO Power Systems
302 Nichols Drive
Hutchins, TX 75141
Attn: R. L. Henry

Arizona Public Service Company
P.O. Box 21666
Phoenix, AZ 85036
Attn: E. Weber

Babcock and Wilcox (3)
91 Stirling Avenue
Barberton, OH 44203
Attn: G. Grant
M. Seale
D. C. Smith

Bechtel Group, Inc.
P. O. Box 3965
San Francisco, CA 94119
Attn: P. DeLaquil
S. Fleming

Black & Veatch Consulting Engineers (2)
P.O. Box 8405
Kansas City, MO 64114
Attn: J. C. Grosskreutz
S. L. Levy

Boeing Aerospace
Mailstop JA-83
P. O. Box 1470
Huntsville, AL 35807
Attn: W. D. Beverly

California Energy Commission
1516 Ninth St., M/S 40
Sacramento, CA 95814
Attn: A. Jenkins

California Public Utilities Com.
Resource Branch, Room 5198
455 Golden Gate Ave.
San Francisco, CA 94102
Attn: T. Thompson

Combustion Engineering, Inc.
1000 Prospect Hill Road
Winsor, CT 06095
Attn: C. R. Buzzuto

El Paso Electric Company
P.O. Box 982
El Paso, TX 79946
Attn: J. E. Brown

Electric Power Research Institute (2)
P.O. Box 10412
Palo Alto, CA 94303
Attn: J. Bigger
E. DeMeo

Elliott, S. D.
1801 Highway 128
Star Route 7550
Philo, CA 95466

Energy Systems Ventures, Inc. (2)
999 Town & Country Road
Orange, CA 92668
Attn: R. L. Gervais
R. Riedesel

Exxon Enterprises, Inc.
P.O. Box 592
Florham Park, NJ 07932
Attn: T. L. Guckes

Foster Wheeler Development Corp.
12 Peach Tree Hill Road
Livingston, NJ 07039
Attn: R. J. Zoschak

Georgia Institute of Technology
Engineering Experiment Street
Atlanta, GA 30332
Attn: C. T. Brown

IEA/SSPS Project
Apartado 649
Almeria, Spain
Attn: C. Arano

Jet Propulsion Laboratory
4800 Oak Grove Drive
Pasadena, CA 91103
Attn: M. Alper

Los Angeles Department of Water and Power
Alternate Energy Systems
P.O. Box 111
111 North Hope St.
Los Angeles, CA 90051
Attn: D. Chu

Martin Marietta Aerospace
P.O. Box 179, MS L0450
Denver, CO 80201
Attn: H. Wroton

Meridian Corporation
5113 Leesburg Pike
Falls Church, VA 22041
Attn: R. King

Olin Chemicals Group (2)
120 Long Ridge Road
Stamford, CT 06904
Attn: F. N. Christopher
L. C. Fiorucci

Pacific Gas and Electric Company
77 Beale Street
San Francisco, CA 94105
Attn: R. E. Price

Pacific Gas and Electric Company (2)
3400 Crow Canyon Road
San Ramon, CA 94526
Attn: G. Braun
J. Iannucci
C. Weinberg

Pioneer Mill Company (AMFAC)
P.O. Box 727
Lahaina, HI 96761
Attn: R. K. MacMillan

Rockwell International
Energy Systems Group
8900 De Soto Avenue
Canoga Park, CA 91304
Attn: T. Springer

Rockwell International
Rocketdyne Division
6633 Canoga Avenue
Canoga Park, CA 91304
Attn: J. Friefeld

Sandia Solar One Office
P. O. Box 366
Daggett, CA 92327
Attn: A. Snedeker

Solar Energy Industries Association
Suite 503
1717 Massachussetts Ave., N.W.
Washington, D.C. 20035
Attn: C. LaPorta

Solar Energy Research Institute (3)
1617 Cole Boulevard
Golden, CO 80401
Attn: B. Gupta
D. Hawkins
R. Hulstram

Southern California Edison
P.O. Box 325
Daggett, CA 92327
Attn: C. Lopez

Southern California Edison (31)
P.O. Box 800
Rosemead, CA 92807
Attn: J. N. Reeves
P. Skvarna (30)

Stearns Catalytic Corp.
P.O. Box 5888
Denver, CO 80217
Attn: W. R. Lang

Stone and Webster Engineering Corporation
P.O. Box 1214
Boston, MA 02107
Attn: R. W. Kuhr

Westinghouse Electric Corporation
Advanced Energy Systems Division
P.O. Box 10864
Pittsbugh, PA 15236
Attn: J. R. Maxwell

E. H. Beckner, 6000; Attn: V. Dugan, 6200
D. G. Schueler, 6220
J. V. Otts, 6222
J. T. Holmes, 6226
R. S. Claassen, 8000; Attn: E. E. Ives, 8100
A. N. Blackwell, 8200
D. L. Hartley, 8300
R. J. Kee, 8245
W. S. Winters, 8245 (5)
R. C. Wayne, 8400; Attn: L. D. Bertholf, 8430
H. Hanser, 8440
R. L. Rinne, 8470
S. E. Faas, 8471 (5)
A. C. Skinrood, 8471 (25)
D. N. Tanner, 8471

Publications Division 8265, for TIC (30)
Publications Division 8265/Technical Library Processes Division, 3141
Technical Library Processes Division, 3141 (3)
P. Dean, 8024, for Central Technical Files (3)